CDF/ANAL/TOP/CDFR/9873
Version 1.1
September 25, 2009

Measurement of the $t\bar{t}$ production cross section in the MET+jets channel with $2.2\ fb^{-1}$ of data

Gabriele Compostella[1]
INFN-CNAF & University of Padova
Silvia Amerio, Donatella Lucchesi
University of Padova

Abstract

In this note we will describe the measurement of the $t\bar{t}$ production cross section in the $\not\!\!E_T + jets$ final state, using a Neural Network to isolate the decay channel. We will show how this choice guarantees a high acceptance to general leptonic W decays, with a sizeable presence of $\tau + jets$ top pair decays, that are very difficult to isolate by means of the standard τ identification procedure. Moreover $\not\!\!E_T + jets$ $t\bar{t}$ decays provide complementary results with respect to standard lepton+jets, di-lepton, and all-hadronic top pair searches: in fact the signal sample we will extract is by means of our choice of cuts orthogonal to the ones used by any other cross section analysis produced so far by the collaboration. This allows us to obtain a measurement that is expected to have a strong impact on the combination of the results produced by the CDF experiment. The analysis reported in this note is based on 2.2 fb^{-1} of data collected up to August 2007 by the TOP_MULTI_JET trigger. After a set of clean-up cuts, a neural network is used to discriminate the $t\bar{t}$ events from the background. After the requirement of at least one jet b-tagged by SECVTX, the cross section is extracted by means of a counting experiment on the sample of data whose neural network output is greater than 0.8. The background in the final selected sample is estimated by means of a b-tagging matrix built on data events (*method-1* approach).

The resulting $t\bar{t}$ production cross section, assuming $M_{top} = 172.5\ GeV/c^2$, is:

$$\begin{aligned} \sigma_{t\bar{t}} &= 7.99\ \pm 0.55\ (\text{stat})\ \pm 0.76\ (\text{syst})\ \pm 0.46\ (\text{lumi})\ pb \\ &= 7.99\ \pm 1.05\ pb \end{aligned}$$

[1]compostella@pd.infn.it

Contents

1 Introduction **3**

2 Datasets **3**
2.1 Data . . . 3
2.2 Monte Carlo . . . 4

3 Trigger simulation **5**

4 Event cleanup **6**

5 Background determination **7**
5.1 *b*-tagging rate parameterization . . . 9
5.2 *b*-tagging matrix . . . 12
5.3 *b*-tagging matrix checks . . . 13
5.3.1 Iterative correction for the presence of top . . . 14
5.3.2 Kinematical distributions of matrix-predicted background . . . 14
5.3.3 *b*-tagging rate extrapolation at high jet multiplicities . . . 15

6 Top Events selection **15**
6.1 Neural Network training . . . 15
6.2 Neural Network performances . . . 20
6.2.1 *b*-tagging rate extrapolation and Neural Network . . . 24

7 Systematic Errors **26**
7.1 Background prediction systematic . . . 26
7.2 Luminosity systematic . . . 26
7.3 Monte Carlo generator dependent systematics . . . 27
7.4 PDF-related systematics . . . 28
7.5 ISR/FSR-related systematics . . . 28
7.6 Systematics due to the jet energy response . . . 30
7.7 *b*-tagging scale factor systematics . . . 31
7.8 Color reconnection systematics . . . 31
7.9 Trigger systematics . . . 31

8 NN cut optimization **38**

9 Cross Section Measurement **40**

10 Summary **44**

11 Bibliography **45**

1 Introduction

In $p\bar{p}$ collisions at $\sqrt{s} = 1.96\ TeV$ top quark pairs are produced through $q\bar{q}$ annihilation ($\sim 85\%$) and gluon fusion ($\sim 15\%$). Since $|V_{tb}| \sim 1$ and $M_t > M_W + M_b$, the $t \to W^+ b$ decay is dominant (and has branching ratio $\sim 100\%$ in Standard Model); so we can classify the different top quark pairs search channels with respect to the W boson decay modes. When both the produced W bosons decay into $e\bar{\nu}_e$ (*or c.c.*) or $\mu\bar{\nu}_\mu$ (*or c.c.*) we have the so called "di-lepton" channel; if both W bosons decay into quark pairs, the final state is instead called "all-hadronic". If one W decays hadronically and the other one leptonically, we have the "lepton+jets" channel.

In this note we describe the measurement of the the $t\bar{t}$ production cross section in the $\not\!\!E_T + jets$ final state, using a Neural Network (NN) to isolate the decay channel. The $\not\!\!E_T + jets$ decay channel has a signature characterized by large jet multiplicity, large missing transverse energy from neutrinos and at least one jet identified as a product of the decay of a b-quark (b-tagged jet). The search for this signature makes the measurement sensitive to W leptonic decays regardless of the lepton type and has a large acceptance with respect to the $W \to \tau\nu$ decays, very difficult to isolate with the standard τ identification tools. The search focuses on the missing transverse energy from the neutrino rather than on lepton identification, and thus it gives complementary and independent results with respect to the "lepton+jets" channel; moreover, with appropriate cuts on the $\not\!\!E_T$, the measurement is also independent from the "all-hadronic" one. The impact on the combined cross section measurement is thus greatly enhanced.

The analysis starts with a series of clean-up cuts in order to perform a first raw selection of events with high $\not\!\!E_T$ and jet multiplicity. A NN is then used to discriminate the signal from the background, mainly composed by QCD and $W/Z+$ heavy flavour jets events. A cut on the NN output selects the final sample, and the cross section measurement is extracted by means of a counting experiment on the number of SECVTX b-tagged jets in the selected events. The background in the final sample is estimated using a *method 1* approach: a matrix is built on data to assign each jet in the final sample the probability to have been produced by a b-quark coming from a background process.

In the following section we will describe in detail all the analysis steps: first the choice of the datasets, the clean-up cuts and the background parametrization. Then we will move to the description of the neural network training and performances. Then the systematic uncertainties affecting the measurement will be described, to conclude with the cross section determination.

2 Datasets

2.1 Data

Several among the available CDF datasets can contain a detectable amount of $\not\!\!E_T + jets$ $t\bar{t}$ events and, in principle, many of the available trigger paths could be used to select

a data sample in which to perform the analysis.

Our choice was to use the TOP_MULTI_JET trigger, which is specifically designed for the all hadronic $t\bar{t}$ decays, whose final state nominally consists of six hadronic jets. The trigger requirements are the following:

- at Level 1 (L1): at least one calorimetric tower with $E_T \geq 10\ GeV$ (from Run 210012 $E_T \geq 20\ GeV$);
- at Level 2 (L2): at least four calorimetric clusters with $E_T \geq 15\ GeV$ each plus a total $\sum E_T \geq 125\ GeV$ (from Run 194328 $\sum E_T \geq 175\ GeV$);
- at Level 3 (L3): at least four jets with $E_T \geq 10\ GeV$.

This choice of trigger is mainly due to the analysis strategy we want to deploy: this "multijet" trigger contains the signal signature we are looking for and gives us the possibility of investigating a sample of events that are normally not used by other analyses, providing a cross section determination uncorrelated with the remaining ones at CDF. Moreover, we will rely on the SECVTX b-tagging algorithm to indentify heavy flavour jets due to top quark decay: for this reason, triggers using selections based on SVT tracks with large impact parameter are not suitable for our purpose, since they can enrich the heavy flavour fraction of the data sample at the cost of introducing a sizeable and difficult to model bias as far as the b-tagging algorithm is concerned. Additionally, triggers with explicit missing E_T requirements can reduce the initial background amount in the triggered data sample, but they enhance the EWK+jets component with respect to the QCD-dominated fraction of events, which is essential to parameterize background b-tagging rates, as will be described in Sec. 5.1.

For these reasons, our choice is to use the TOP_MULTI_JET trigger which provides, at the first order, a QCD-dominated sample in which background prediction tools can be developed and used to estimate the background to $\not\!\!E_T + jets\ t\bar{t}$ decays.

The results reported in this work are based on data collected from March 2002 to August 2007. With the requirement of fully operational silicon detectors, calorimeters and muon systems[2], the total integrated luminosity used in the analysis and corresponding to this period is 2.2 fb^{-1}. Additional details about the datasets used in this analysis are reported in Tab. 1.

2.2 Monte Carlo

The signal events are simulated using the *ttop25* dataset, generated using PYTHIA with $M_{top} = 172.5\ GeV/c^2$. For the evaluation of the systematic uncertainties (see Section 7) we used the following samples:

- *dtopa2* and *dtopa3* (HERWIG) for the systematics on the MC generator;

[2]Good run list v26 "em_mu_si_cmxignored".

Dataset	Run Range	CDF code version	Lum. (nb^{-1})
gset0d	138425 - 186598	prod 5.3.1 - topCode 6.1.4	326671
gset0h	190697 - 203799	prod 6.1.1 - topCode 6.1.4	356320
gset0i	222529 - 228596	prod 6.1.1 - topCode 6.1.4	572150
gset0j	228664 - 246231	prod 6.1.1 - topCode 6.1.4	911217
			tot. 2166358

Table 1: CDF datasets used for this analysis. The table shows the available run range and the version of the production and reconstruction software. Offline luminosity is still not corrected by the factor of 1.019.

- *dtops1* and *dtops2* (PYTHIA) for ISR/FSR systematic error;
- *ctopse* and *ctopsd* (PYTHIA) for color reconnection systematic error.

3 Trigger simulation

The TOP_MULTI_JET trigger requirements have been revised during data taking to cope with Tevatron increasing luminosity. The data used in this analysis are collected with three versions of the trigger, differing for L1 and L2 requirements:

- Runs *138425-195408* (*p0-p1*): at L1 at least one calorimetric tower with $E_T >$ 10 GeV, at L2 four clusters with $E_T > 15$ GeV and $\Sigma E_T > 125$ GeV;
- Runs *195409-212133* (*p2-p7*): at L1 at least one calorimetric tower with $E_T >$ 10 GeV, at L2 four cluster with $E_T > 15$ GeV and $\Sigma E_T >$ **175 GeV**;
- Runs *217990-246231* (*p8-p13*): at L1 at least one calorimetric tower with $E_T >$ **20 GeV**, at L2 four clusters with $E_T > 15$ GeV and $\Sigma E_T > 175$ GeV;

L3 requirement was always the presence of at least four jets with $E_T \geq 10\ GeV$.

In order to work on a uniform sample of data, we decided to simulate the new L2 requirement of $\Sigma E_T > 175$ GeV on the events taken before $p2$.

On all MC samples, instead, we will perform a full simulation of the trigger path using the scale factors computed by A.Mitra [1] in order to correct the L2 cluster transverse energy for a bug in the CDF code used for MC simulation.

Since no information on L1 is available in the MC TopNtuples we used for our analysis, we need a way to simulate correctly the L1 requirements on MC events. Previous studies [2] show that the requirement of L1_JET10 is 99% efficient when TOP_MULTI_JET L2 with $\Sigma E_T > 175$ GeV is fired, so we can safely choose not to simulate the L1_JET10 requirement on MC events corresponding to runs before p8.

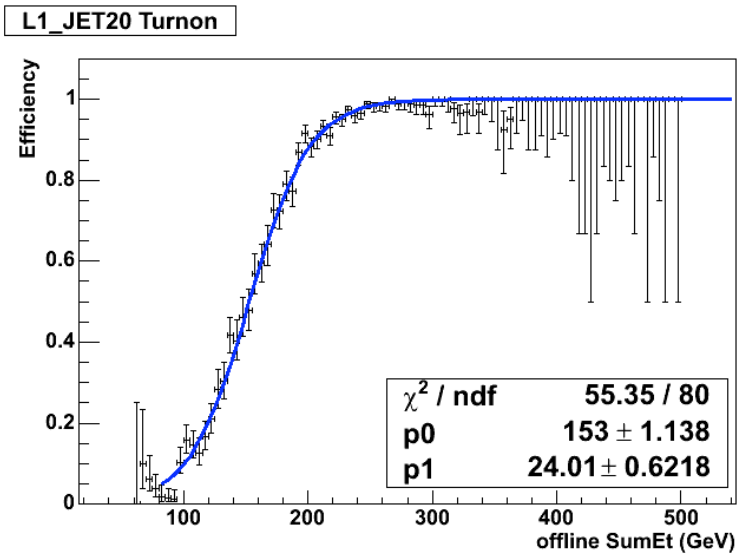

Figure 1: L1_JET20 rate versus offline SumEt, L5 corrected, derived from Tower10 dataset, together with its fit. See text for details.

In order to simulate correctly the requirement of L1_JET20 on MC events corresponding to runs after p8, we derive a turnon function from Single Tower 10 dataset. Tower10 dataset is collected using the following trigger requirements:

- at Level 1 (L1): at least one calorimetric tower with $E_T \geq 10\ GeV$;
- at Level 2 (L2): a static prescaling factor of 1K;
- at Level 3 (L3): auto-accept.

Using this data sample we derive the turnon $N_{L1\&\&L2}(SumEt)/N_{L2}(SumEt)$, where $N_{L1\&\&L2}(SumEt)$ is the number of events in the sample vs offline SumEt L5 corrected that have fired both L1_JET20 and TOP_MULTI_JET L2 with $\Sigma E_T > 175$ GeV, while $N_{L2}(SumEt)$ is the number of events in the sample vs offline SumEt L5 corrected that have fired TOP_MULTI_JET L2 with $\Sigma E_T > 175$ GeV. The turnon obtained using this procedure is shown in Fig. 1, together with the sigmoid function used to fit it.

We will use the fit of the turnon to reweigh MC events passing the TOP_MULTI_JET L2 simulation and corresponding to runs after p8. This introduces a correction of order $\sim 4\%$ in the simulated L2 trigger efficiency.

4 Event cleanup

The following prerequisites are applied both to data and Monte Carlo samples before any kinematical selection:

- we consider Good run list *v26 em_mu_si_cmxignored*

- we discard events whose primary vertex location is not well centered in the CDF II detector, in particular:
  - In order to select well centered events, the z coordinate of the highest-$\sum P_T$ good quality vertex is required to be within ± 60 cm from the geometrical center of the detector: $|z_{vert}| < 60$ cm.
  - We require that the vertex used for jet reclustering and then for the secondary vertex search is close to be the primary vertex found in the event by means of the *PrimVtx*. So we require the distance between the event primary vertex and the vertex used for jet reclustering $|z_{jet} - z_{primvtx}|$ to be less than 5 cm, where z_{jet} denotes the z_0 of the good quality highest-P_T vertex.
  - A good quality vertex, by definition, is formed with at least three COT tracks [3]. We require the number of good quality vertices in the event to be greater than zero.
- We simulate the new $L2$ $\Sigma E_T > 175$ GeV trigger requirement on data taken before run 194328, to have an homogenous sample to perform our analysis.
- When dealing with Monte Carlo events, we perform a full simulation of the TOP_MULTI_JET trigger path using for $L2$ $\Sigma E_T > 175$ GeV and weighing events by the L1_JET20 rate if necessary.
- We reject events with a good, $high - P_T$ reconstructed electron or muon to avoid overlaps with other top lepton+jets analyses.
- We clean up our sample by requiring events to have at least 3 *tight* jets, i.e. jets with $E_T^{L5} \geq 15$ GeV and $|\eta| \leq 2.0$.
- We reject events with low $\not\!\!E_T$ by requiring $\not\!\!E_T{}^{sig} \geq 3$ $GeV^{1/2}$, thus avoiding overlaps with top all-hadronic analyses.

The impact of these preliminary selections on data and inclusive Monte Carlo $t\bar{t}$ is shown in Tab. 2, 3 and 4. After prerequisites application we expect a signal to background ratio S/B of 1.0% in the sample with $NJets \geq 3$, of 0.1% in the sample with exactly 3 tight jets and of 1.4% in the sample with $NJets \geq 4$.

5 Background determination

Our measurement will be performed counting the number of jets b-tagged by the SECVTX algorithm. In order to derive a cross section measurement from the final tagged sample we need to find an estimate of the number of b-tagged jets yielded by background processes.

N evts	gset0d	gset0h	gset0i	gset0j	tot.
Good Run	4466188	2674058	3349900	4414134	14904280
Trigger	1167368	1744704	3349899	4414134	10676105
$\|Z_{vert}\| < 60\ cm$	1091891	1527136	3018242	4144055	9781324
$\|Z_{jet} - Z_{primvtx}\| < 5\ cm$	1059897	1433601	2877148	3845855	9216501
N_{vert} good quality ≥ 1	1059896	1433601	2877148	3845855	9216500
N tight leptons = 0	1058342	1431754	2872926	3841620	9204642
NJets ≥ 3	1023215	1341713	2806210	3614881	8786019
$\not\!\!E_T{}^{sig} \geq 3\ GeV^{1/2}$	13496	20699	38919	65413	138527
Out of which:					
with NJets= 3	3922(0.1%)	7815(0.3%)	9529(0.3%)	23044(0.5%)	44310(0.3%)
with NJets$\geq$ 4	9574(0.2%)	12884(0.5%)	29390(0.9%)	42369(1.0%)	94217(0.6%)

Table 2: Events surviving the clean-up requirements for data, divided in each period of data taking.

Rel. Eff. (%)	gset0d	gset0h	gset0i	gset0j	tot.
Good Run	100	100	100	100	100
Trigger	26.1	65.3	100	100	71.6
$\|Z_{vert}\| < 60\ cm$	93.5	87.5	90.1	93.9	91.6
$\|Z_{jet} - Z_{primvtx}\| < 5\ cm$,	97.1	93.9	95.3	92.8	94.2
N_{vert} good quality ≥ 1	100	100	100	100	100
N tight leptons = 0	99.9	99.9	99.9	99.9	99.9
NJets ≥ 3	96.7	93.7	97.7	94.1	95.4
$\not\!\!E_T{}^{sig} \geq 3\ GeV^{1/2}$	1.3	1.5	1.4	1.8	1.6

Table 3: Relative efficiency of the clean-up requirements for data, divided in each period of data taking.

In the following we will describe a procedure to obtain a reliable prediction of the total amount of b-tags coming from background events, which will then be a part of the neural network selection optimization procedure on the data sample. Given our tight prerequisite cut on $\not\!\!E_T/\sqrt{\Sigma E_T}$ and the ≥ 1 positive b-tag requirement that will be enforced on the final sample, we expect the main background contributions to come from events like $b\bar{b} + jets$ and $Wb\bar{b} + jets$ [7].

In order to determine the background parameterization, the complete data sample after the clean-up cuts can not be directly used since it has a sizeable signal contamination. Making the assumption that the per-jet positive tagging rate does not depend on the number of jets in the event, we will limit ourselves to the subsample of events with exactly 3 *tight* jets (i.e. jets with $E_T \geq 15\ GeV$ and $|\eta| \leq 2.0$), where the $t\bar{t}$ fraction is negligible, and we will use this background-dominated sample to derive a

N evts	MC_{incl}	Rel. eff.(%)	Abs. eff.(%)	evts in 2.2 fb^{-1}
Good Run	4787475	100	100	16390
$\|Z_{vert}\| < 60\ cm$	4580599	95.7	95.7	15682
Trigger	2446149	53.4	51.1	8374
$\|Z_{jet} - Z_{primvtx}\| < 5\ cm$	2442174	93.8	51.0	8361
N_{vert} good quality ≥ 1	2442174	100	51.0	8361
N tight leptons = 0	2199776	90.1	46.0	7531
NJets ≥ 3	2199302	99.9	46.0	7529
$\not\!\!E_T{}^{sig} \geq 3\ GeV^{1/2}$	396924	18.0	8.3	1359
Out of which:				
with NJets= 3	9087	2.3	0.2	31
with NJets$\geq$ 4	387837	97.7	8.1	1328

Table 4: Events surviving the clean-up requirements for inclusive Monte Carlo $t\bar{t}$ samples. Last column shows the amount of $t\bar{t}$ events expected in 2.2 fb^{-1} of data assuming $\sigma_{t\bar{t}} = 7.45$ pb.

per-jet b-tagging probability parameterization for events that are not top-like. We will then check the parameterization predictions for higher jet multiplicities and use it for the background determination in the neural network selected sample.

5.1 b-tagging rate parameterization

The basic idea of our background prediction method rests on the assumption that b-tag rates for $t\bar{t}$ signal and background processes show differences that are due to the different properties of the b-jets produced by the top quark decays compared to the b-jets arising from QCD and vector boson plus heavy flavour production processes. In this hypothesis, parameterizing the b-tag rates as a function of some chosen jet characteristics, in events depleted of signal contamination, will allow to predict the number of b-tagged jets from background processes present in a given selected sample.

We summarize below the steps needed for this approach:

1. identify a subsample of data with negligible $t\bar{t}$ contamination;

2. in the identified sample, parameterize the b-tagging rate as a function of the N variables on which it mainly depends.

3. Build a N-dimensional b-tagging matrix in order to associate to a given jet a probability to be identified as a b-jet given its characteristics.

4. Predict the total amount of expected background tags in a given sample by summing b-tagging probabilities over all jets in the selected events.

5. In samples depleted of signal, check the matrix background prediction by comparing the number of expected and observed SECVTX tagged jets.

6. Use the tagging matrix to calculate the amount of background tags in the sample to be used for the cross section measurement.

We remind that the use of this method based on tagging rate parameterizations rests on the assumption that the sample used for b-tag rates dependencies studies shows a negligible $t\bar{t}$ contamination: a $t\bar{t}$ presence in the sample used to parameterize the tagging rate may have a sizable impact in the amount of background tags prediction. For this reason, we need to choose as base sample a data region depleted as much as possible of signal: in our case, we decide to use for the background tagging rate parameterization the data sample obtained after the prerequisites application with exactly 3 tight jets (i.e. jets with $E_T^{L5} \geq 15\ GeV, |\eta| \leq 2.0$).

Tab. 5 show the number of events in the data sample and the $t\bar{t}$ contamination expected from Monte Carlo assuming the theoretical production cross section of 7.45 pb, corresponding to a top mass of $M_{top} = 172.5\ GeV/c^2$ for different tight jet multiplicities.

Number of Events	3 jets	4 jets	5 jets	6 jets	7 jets	8 jets
Data	44,310	52,691	22,760	9,871	2,714	660
$t\bar{t}$ MC	9,090	107,938	152,740	87,342	30,074	7,789
Exp. $t\bar{t}$ in 2.2 fb^{-1}	31	371	524	300	103	27
Exp. Contamination (%)	0.07	0.7	2.31	3.04	3.81	4.05

Table 5: Expected signal contamination for different jet multiplicities.

We can define the b-tagging probability as the ratio of the number of positive SECVTX tagged jets to the number of taggable jets in the sample of data events after prerequisites with exactly 3 jets, where we define as taggable a tight jet (with $E_T^{L5} \geq 15\ GeV$, and $|\eta| < 2.0$) with at least two good SECVTX tracks.

The per-jet b-tagging probability has been parameterized as a function of several jet and event variables in order to extract its main dependencies, and is found to depend mainly on jet characteristics such as E_T, the number of good quality tracks contained in the jet cone N_{trk}, and the $\not\!\!E_T$ projection along the jet direction $\not\!\!E_T{}^{prj}$, defined by:

$$\not\!\!E_T{}^{prj} = \not\!\!E_T \cos\Delta\phi(\not\!\!E_T, jet). \tag{1}$$

Figure 2 shows both the positive and negative tagging rates dependence on the set of variables chosen to parametrize the tagging probability.

Jet E_T and N_{trk} correlation with the tagging probability is expected due to the implementation details of the b-tagging algorithm. The $\not\!\!E_T$ projection along the jet direction is instead correlated with the heavy flavour component of the sample [6, 7] and with the geometrical properties of the event: in fact b-quarks can yield a considerable

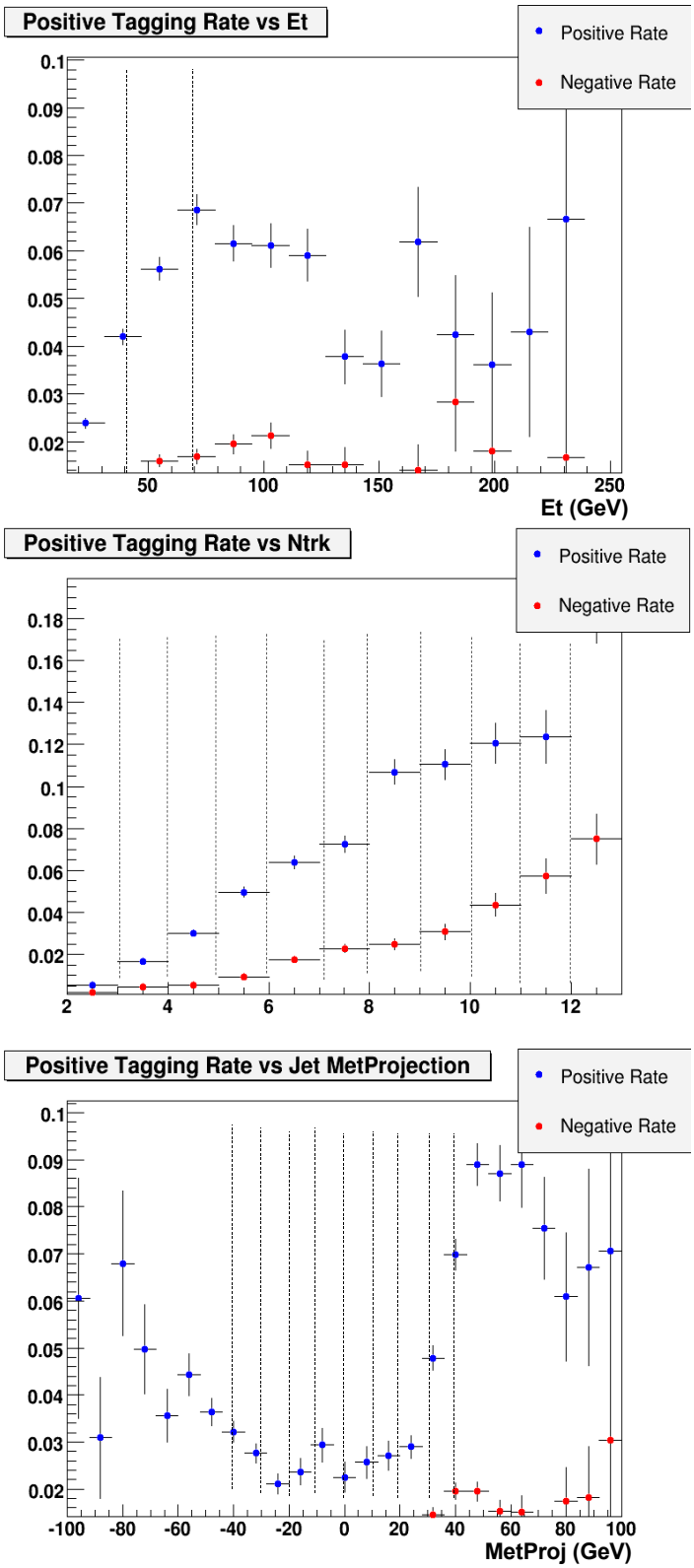

Figure 2: Positive and negative b-tagging rates as a function of E_T, N_{trk} and $\not\!\!E_T{}^{prj}$ for the data sample with exactly 3 tight jets in the event. The dotted vertical lines represent the binning used in the matrix parametrized with these variables.

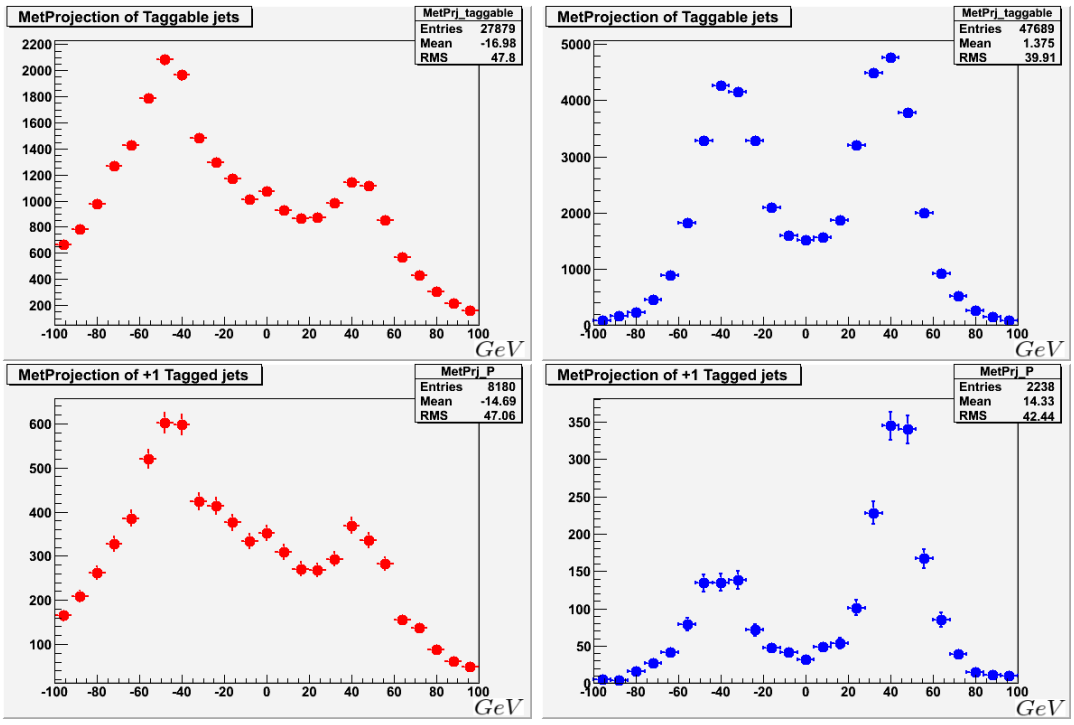

Figure 3: $\not\!\!E_T{}^{prj}$ distribution for inclusive Monte Carlo $t\bar{t}$ and data 3-jet events. Top row: left (right) $\not\!\!E_T{}^{prj}$ plot for taggable jets in $t\bar{t}$ (data). Second row: missing transverse energy projection for positive tagged jets for both $t\bar{t}$ (left) and data (right).

amount of missing transverse energy due to their semi-leptonic decays and in that case the $\not\!\!E_T$ is expected to be aligned with the jet direction; on the contrary, $\not\!\!E_T$ produced in W boson decays stands more likely away from jets, depending on the process-allowed regions of the phases space. By requiring the events to have large missing E_T significance ($\not\!\!E_T/\sqrt{\Sigma E_T} \geq 3\ GeV^{1/2}$) as an analysis prerequisite, we reject those events whose missing E_T is mainly due to residual energy mis-measurement effects, and in turn concentrate our attention on physics-induced $\not\!\!E_T$.

These $\not\!\!E_T{}^{prj}$ features are depicted in Fig. 3. The upper left plot of Fig. 3 shows the $\not\!\!E_T{}^{prj}$ for taggable jets in 3-jet inclusive Monte Carlo $t\bar{t}$ events. On the other hand, in the upper right plot the corresponding distribution extracted from 3-jet events in multijet data is shown for comparison. On the second row, the missing transverse energy projection is drawn for SECVTX positive tagged jets, for both the samples.

5.2 b-tagging matrix

Now we can define a so-called b-tagging matrix, using the per-jet b-tagging probability dependencies studied previously. The 3-dimensional matrix binning we decided to choose, according to the tagging rate dependencies shown in Fig. 2 and in order to minimize the number of low statistics or undefined matrix bins, is the one that was

already successful in previous analyses:

- 3 bins in jet E_T: [15, 40); [40, 70); $\geq$ 70 GeV;
- 11 bins in jet N_{trk}: from $N_{trk} = 2$ to $N_{trk} \geq 12$;
- 10 bins in $\not\!\!E_T{}^{prj}$: < -40; $[-40, -30)$; $[-30, -20)$; $[-20, -10)$; $[-10, 0)$; $[0, 10)$; $[10, 20)$; $[20, 30)$; $[30, 40)$; and ≥ 40 GeV.

Each jet contained in the 3-jet events data sample will be classified according to the matrix bin it belongs to, in terms of the corresponding jet variables E_T, N_{trk} and $\not\!\!E_T{}^{prj}$. After the classification, for each matrix bin (x, y, z), with x, y, z integers in the range allowed by the chosen matrix binning, the total number of positive b-tagged jets $N^{+}_{jets}(x, y, z)$ and the total number of taggable jets $N^{taggable}_{jets}(x, y, z)$ falling in the (x, y, z) matrix bin will be used to calculate the following tagging rate

$$\mathcal{R}(x, y, z) = \frac{N^{+}_{jets}(x, y, z)}{N^{taggable}_{jets}(x, y, z)} \tag{2}$$

This allows us to associate to each $k-th$ jet in an event a $3-d$ b-tagging probability:

$$\mathcal{P}(E^k_T, N^k_{trk}, \not\!\!E_T{}^k_{prj}) = \mathcal{R}(x, y, z) \tag{3}$$

by finding the (x, y, z) matrix bin corresponding to the $(E^k_T, N^k_{trk}, \not\!\!E_T{}^k_{prj})$ triplet of jet variables.

This per-jet probability will allow to calculate the number of background b-tags expected in a given data sample as follows: the number of expected background b-tags in the $i-th$ event in a given sample, is defined as:

$$N^i_{tags} = \sum_{k=1}^{n} \mathcal{P}(E^k_T, N^k_{trk}, \not\!\!E_T{}^k_{prj}) \tag{4}$$

where the sum on k is over all taggable jets in the event. The total number of tagged jets expected for a given data sample will then be the sum of the expected tags per each event.

In the next section we will check if this choice of parameterization and binning is satisfactory.

5.3 b-tagging matrix checks

Before applying the parameterization we found previously to estimate the number of background b-tagged jets in a given data sample, we first want to check that it can predict the right kinematical distributions for b-tagged events in samples of data before any selection, where the $t\bar{t}$ signal contamination is quite small. Moreover, we will check its prediction as a function of the jet multiplicities. In both cases, as we have to apply the b-tagging matrix to a sample data, we first need to correct for the presence of top events in the sample.

5.3.1 Iterative correction for the presence of top

In general, before applying the tag matrix to a data sample, we have to ensure that the data sample before the tagging requirement contains a negligible $t\bar{t}$ component. If this is not the case, then the tagging rate parameterization procedure will overestimate the background. In fact the expected number of b-tags provided by the positive tagging matrix parameterization will not refer only to background events, since it receives a contribution from $t\bar{t}$ events in the pre-tagging sample.

We can correct for this effect by removing the $t\bar{t}$ contribution in the sample in order to have a background-only determination of the number of expected b-tags. To do so, we iteratively correct the number of expected b-tags in the sample as follows [8]:

$$N'_{exp} = N^{fix}_{exp}\frac{N_{evt} - N^{t\bar{t}}_{evt}}{N_{evt}} = N^{fix}_{exp}\frac{N_{evt} - \frac{N_{obs}-N_{exp}}{\epsilon^{ave}_{tag}}}{N_{evt}} \tag{5}$$

where:

- N^{fix}_{exp} is the number of expected tags coming from the tag rate parameterization before any correction; this number is fixed during the iterative procedure.
- N_{evt} is the number of events in the pre-tagging data sample used to determine N^{fix}_{exp} through the tag matrix prediction;
- ϵ^{ave}_{tag} is the average tagging efficiency, defined as the Monte Carlo ratio between the number of positive b-tagged jets and the number of events in the pre-tag sample;
- $N^{t\bar{t}}_{evt}$ is the $t\bar{t}$ contamination in the pre-tagging sample, estimated as $\frac{N_{obs}-N_{exp}}{\epsilon^{ave}_{tag}}$.

The iterative procedure stops when the difference $|N'_{exp} - N_{exp}| \leq 1\%$.

5.3.2 Kinematical distributions of matrix-predicted background

Once we have chosen our parameterization variables and built the tagging matrix, we can use the matrix definition to construct kinematical distributions and compare them with the observed data distributions for events with $N_{jet}(E^{L5}_T \geq 15\ GeV, |\eta| \leq 2.0) \geq 3$ and at least one b-tagged jet before any other kinematical requirements except the clean-up prerequisites selection.

The matrix-predicted kinematical distributions are obtained by weighting each jet according to its parameterized tagging probability.

Fig. 4 shows the observed and matrix-predicted distribution for kinematical variables such as jet E_T, N_{trk}, $\not\!\!E^{prj}_T$, η, ϕ, then global event variables Aplanarity, Centrality and Sphericity.

Fig. 5 shows the observed and matrix-predicted distribution for another set of kinematical variables such as $\not\!\!E_T$, $\not\!\!E^{sig}_T$, $\sum E_T$, $\sum E^3_T$, the minimum difference in ϕ between

the $\not\!\!E_T$ and each jet in the event $\Delta\phi_{min}$, the number of good quality vertices N_{v12}, luminosity and event run.

The insets at the bottom of each panel display the bin-by-bin ratio of observed to matrix-calculated distributions. In general, the observed to expected ratio is almost flat for all the variables here considered. Exceptions are for example the jet E_T and jet η spectra. For jet E_T the ratio shows some structure at low E_T, in the range $15 \div 40\ GeV$, where the b-tagging rate is parameterized with a single matrix bin. Generally the ratio between observed and expected distributions behaves well, confirming the effectiveness of the tagging matrix in describing the kinematical distribution of tagged data.

5.3.3 b-tagging rate extrapolation at high jet multiplicities

Another important check consists in extrapolating the b-tagging rate dependencies at jet multiplicities higher than 3, where the matrix is parameterized, and compare the b-tags prediction from tagging matrix application to data to the observed number of b-tagged jets. This extrapolation is performed on the complete data sample obtained after the application of the prerequisites but before any additional kinematical requirement.

The results of this approach are shown in Fig. 6, where we assumed a $t\bar{t}$ production cross section $\sigma_{t\bar{t}} = 7.45\ pb$ for the Monte Carlo. The red error bands in the plot are statistical only and come from the tag matrix application: we recall that for each matrix bin, the tag rate is calculated as $N^{+}_{bin}/N^{taggable}_{bin}$ with N^{+}_{bin} being the number of positive tagged jets and $N^{taggable}_{bin}$ the number of taggable jets in that matrix bin in the 3-jets sample used for matrix parameterization. We thus propagate the error associated with this ratio to the expected number of tags.

Once we take into account the $t\bar{t}$ signal contamination in the sample and its contribution to the number of observed b-tags, the agreement between the number of observed and predicted b-tags is good in all the jet multiplicity bins, being exactly the same by definition for 3-jet events, on which the matrix is calculated.

6 Top Events selection

In order to enhance the signal to background ratio in our final sample, we will use a neural network, trained to discriminate $t\bar{t} \rightarrow \not\!\!E_T + jets$ signal events from background.

6.1 Neural Network training

To build our Neural Network (NN) we use the class *TMultiLayerPerceptron* available in ROOT. For what concerns training samples, as background we will use all the data taken with the TOP_MULTI_JET trigger and passing the prerequisites previously discussed; additionally, we will require the presence of at least 4 tight jets in the event (i.e. jets with $E_T^{L5} \geq 15\ GeV$ and $|\eta| \leq 2.0$) to perform the training in a sample completely uncorrelated with the one we used to determine the background

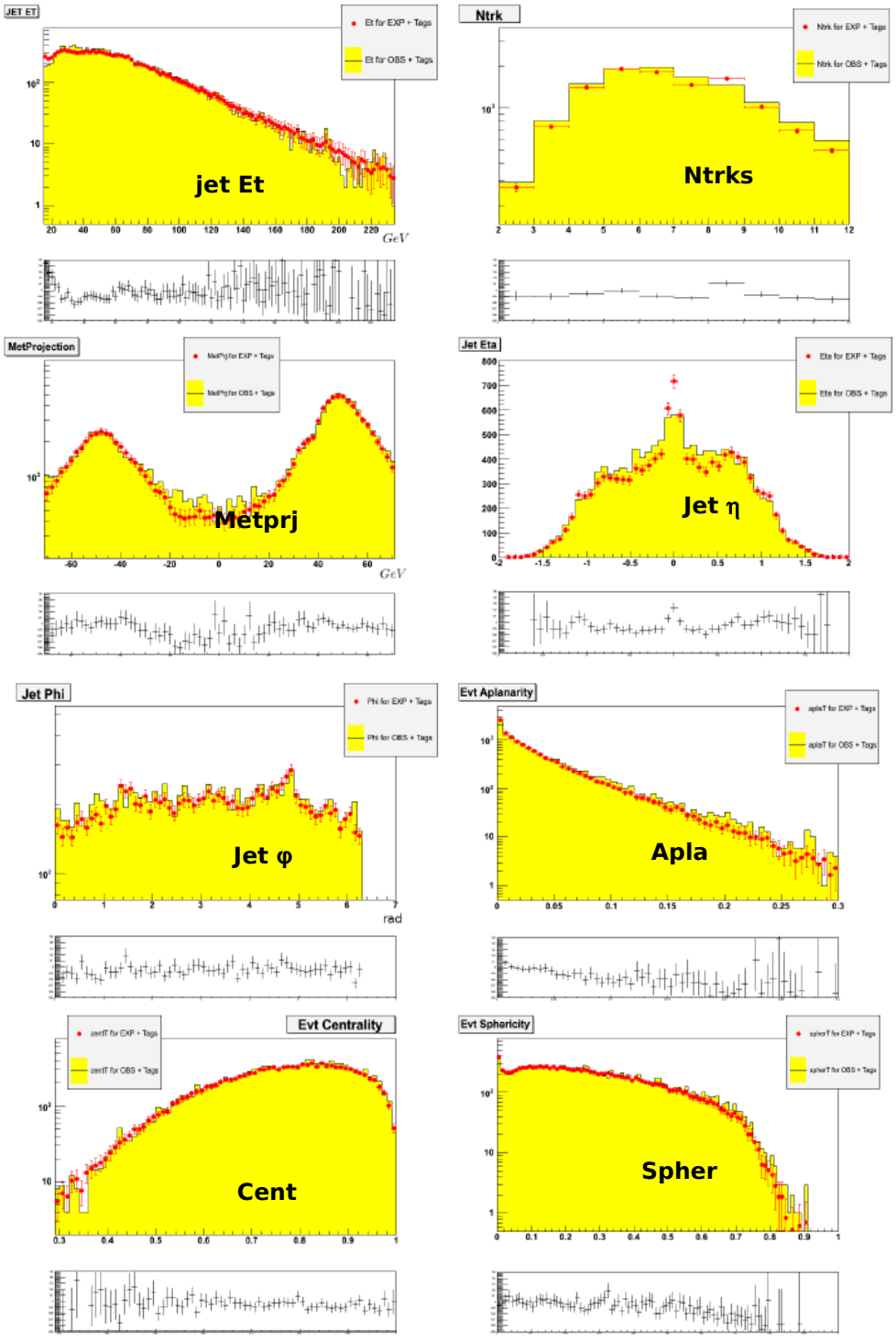

Figure 4: Checks of tagging matrix-based variables distributions in data events with at least three $E_T^{L5} \geq 15\ GeV$ and $|\eta| \leq 2.0$ jets. From top to bottom, from left to right: Jet E_T, N_{trk}, $\not\!\!E_T^{prj}$ η, ϕ; then global event variables Aplanarity, Centrality and Sphericity. All plots except the one for η are in log scale. The insets at the bottom of each panel display the bin-by-bin ratio of observed to matrix-calculated distributions.

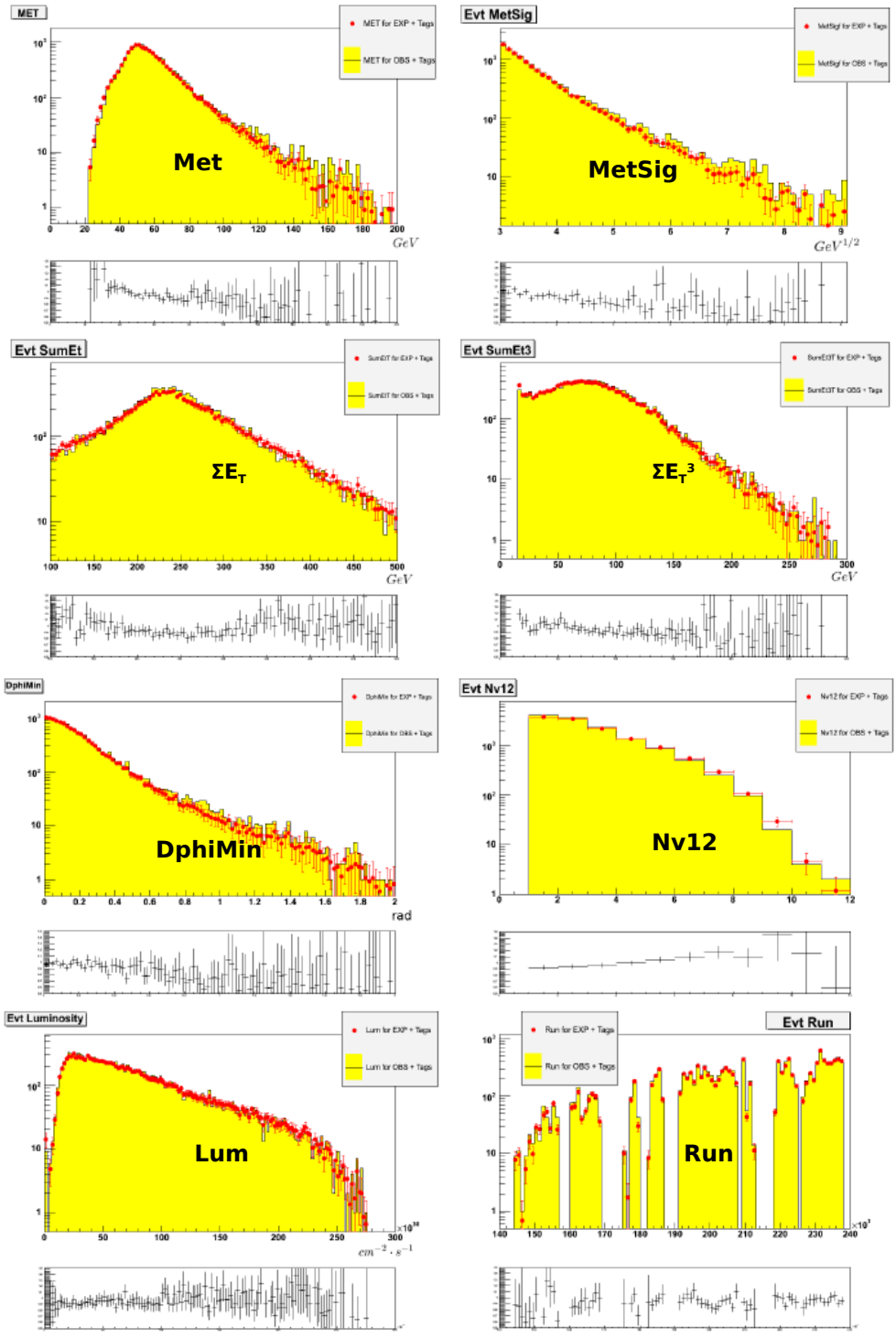

Figure 5: Checks of tagging matrix based event variables distributions in data events with at least three $E_T^{L5} \geq 15\ GeV$ and $|\eta| \leq 2.0$ jets. From top to bottom, from left to right: $\not\!\!E_T$, $\not\!\!E_T^{sig}$, $\sum E_T$, $\sum E_T^3$, $\Delta\phi_{min}$, the number of good quality vertices N_{v12}, luminosity and event run. All plots are in log scale. The insets at the bottom of each panel display the bin-by-bin ratio of observed to matrix-calculated distributions.

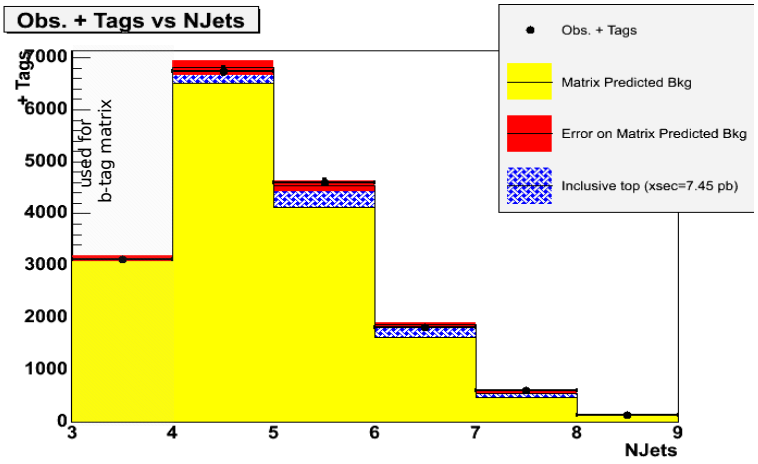

Figure 6: Tagging matrix check after prerequisites application and before any kinematical selection. Observed and predicted positive b-tags as a function of the jet multiplicity. The expected contribution coming from $t\bar{t}$ events is also shown, see text for details.

parameterization. For signal we will use the same amount of events passing the same requirements of the data, taken randomly from the available Monte Carlo sample.

Moreover, in order to further clean up our sample and to select a signal enriched region, we remove events with low angle between jets and $\not\!\!E_T$, $\Delta\phi_{min}$ using an additional cut on $\Delta\phi_{min} > 0.4$ (see Fig. 7). This cut has been choosen following the same approach of the previous analysis in this decay channel [4]; it allows to select a sample with well known and modeled kinematical properties and avoids any possible enhancement by the Neural Network of signal characteristics that can be difficult to model, since events with low angle between jets and $\not\!\!E_T$ in our sample are mainly due to energy mismeasurements.

After applying this cut on Data and MC samples with at least 4 tight jets, we have the following results: on the MC we are left with $207,381$ events, to be compared with $387,837$ events with 4 tight jets before the $\Delta\phi_{min}$ cut (efficiency 53.5%). On Data $20,043$ out of $94,217$ events with 4 tight jets pass the $\Delta\phi_{min}$ cut (efficiency 21.3%).

After these requirements, the signal contamination in the data sample with $NJets \geq 4$ obtained after prerequisites application is $\sim 3.5\%$ (assuming $\sigma_{top} = 7.45\ pb$) and can thus be considered negligible, meaning that we can consider all these data events as background in our neural network training without affecting its rejection power.

We used the topology depicted in Fig. 8, using as inputs for the network the following kinematical variables, normalized with respect to their maximum value:

- E_{T1}, the transverse energy of the leading jet;

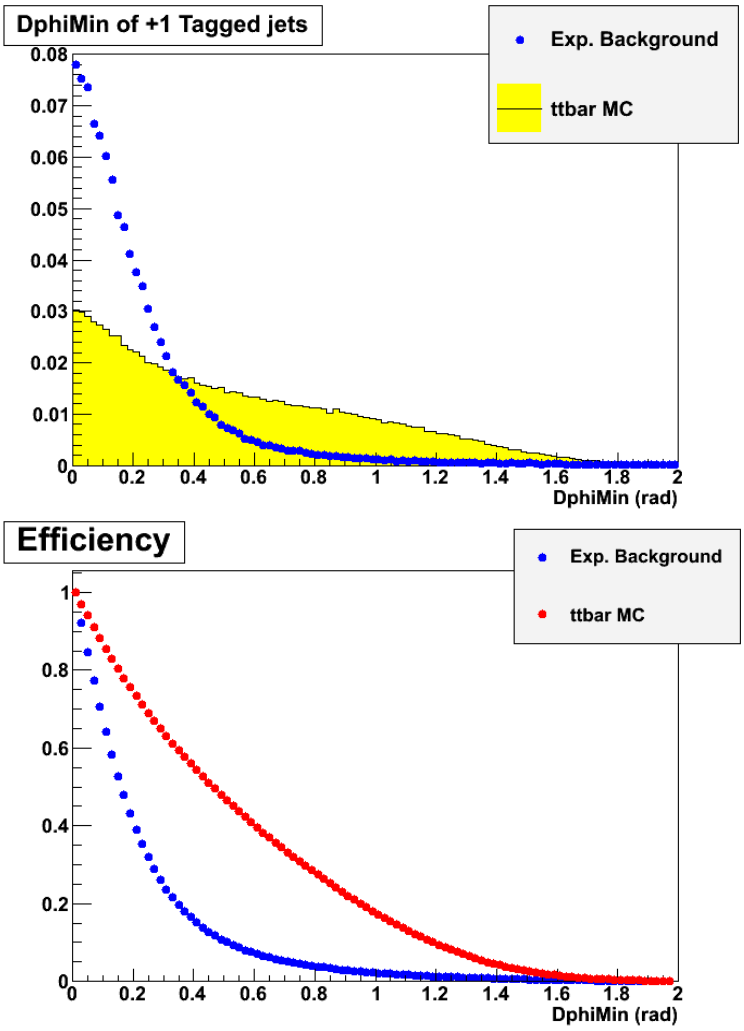

Figure 7: Up: $\Delta\phi_{min}$ distribution for $t\bar{t}$ +1 tagged jets and background matrix predicted +1 tagged jets. In order to remove events affected by energy mismeasurement, we require $\Delta\phi_{min} > 0.4$. Bottom: efficiency of the cut on $\Delta\phi_{min}$ for $t\bar{t}$ +1 tagged jets and background +1 tagged jets, as expected from tag matrix application.

- $\Delta\phi_{min}$, already defined as $\min \Delta\phi(\not\!\!E_T, jet)$, the minimum difference between the $\not\!\!E_T$ and each jet in the event in the ϕ coordinates;
- ${\not\!\!E_T}^{sig}$, the $\not\!\!E_T$ significance of the event, defined as $\not\!\!E_T/\sqrt{\Sigma E_T}$;
- the energy-related variables $\sum E_T$, $\sum E_T^3$ and the Centrality;
- the topology-related variables Sphericity and Aplanarity.

Fig. 9 shows the signal versus background distributions of each input variable going into the network after the application of the previously discussed prerequisites. The

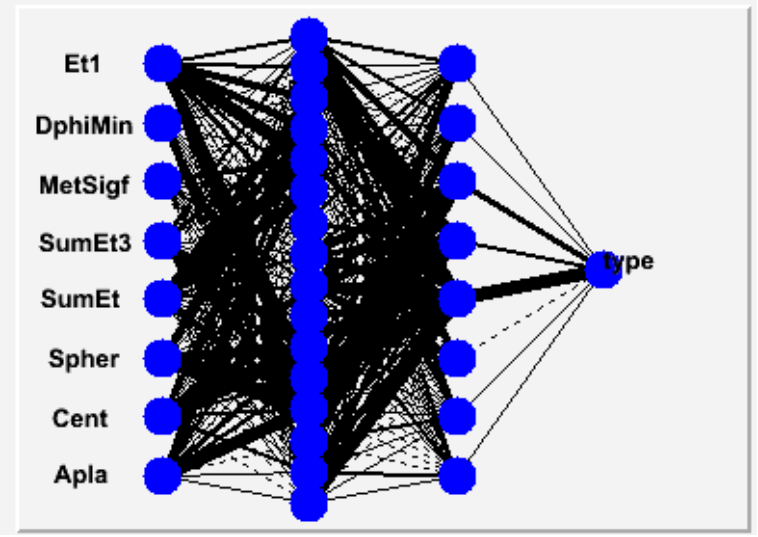

Figure 8: The 8-16-8-1 topology of the network used in the analysis: a feed forward neural network with 2 hidden layers, 8 input nodes and one single output for classification. The thickness of the black lines connecting each perceptron is proportional to the associated weight.

obtained sample made of signal and background events will be split in two parts: half will be used for neural network training and the other half for the so called testing during each iteration of the training procedure; a plot describing the "history" of the training is shown in Fig. 10: for each training epoch the average error made by the network in trying to discriminate events belonging to the signal or background class is calculated both for the events in the training sample and in the test one.

We stop our training pocedure after 200 epochs, since after this number of iterations the network reaches the minimum of the error function for the chosen topology. Additionally, we want to avoid a situation of *overtraining*: overtraining happens when a neural network learns "too well" the details of the training set, getting stuck in the statistical fluctuations of its input variables, and looses the capability of generalizing its results on a different sample. The fact that errors on the training sample and on the test one are almost the same over all the training period tells us that the network has not been overtrained.

6.2 Neural Network performances

The neural network obtained after the training procedure is then applied to all the available events (training + test samples) and its output is shown in Fig. 11: signal and background are well separated and their distributions are well peaked around their expected values.

The performances of the neural network are described in terms of efficiency and

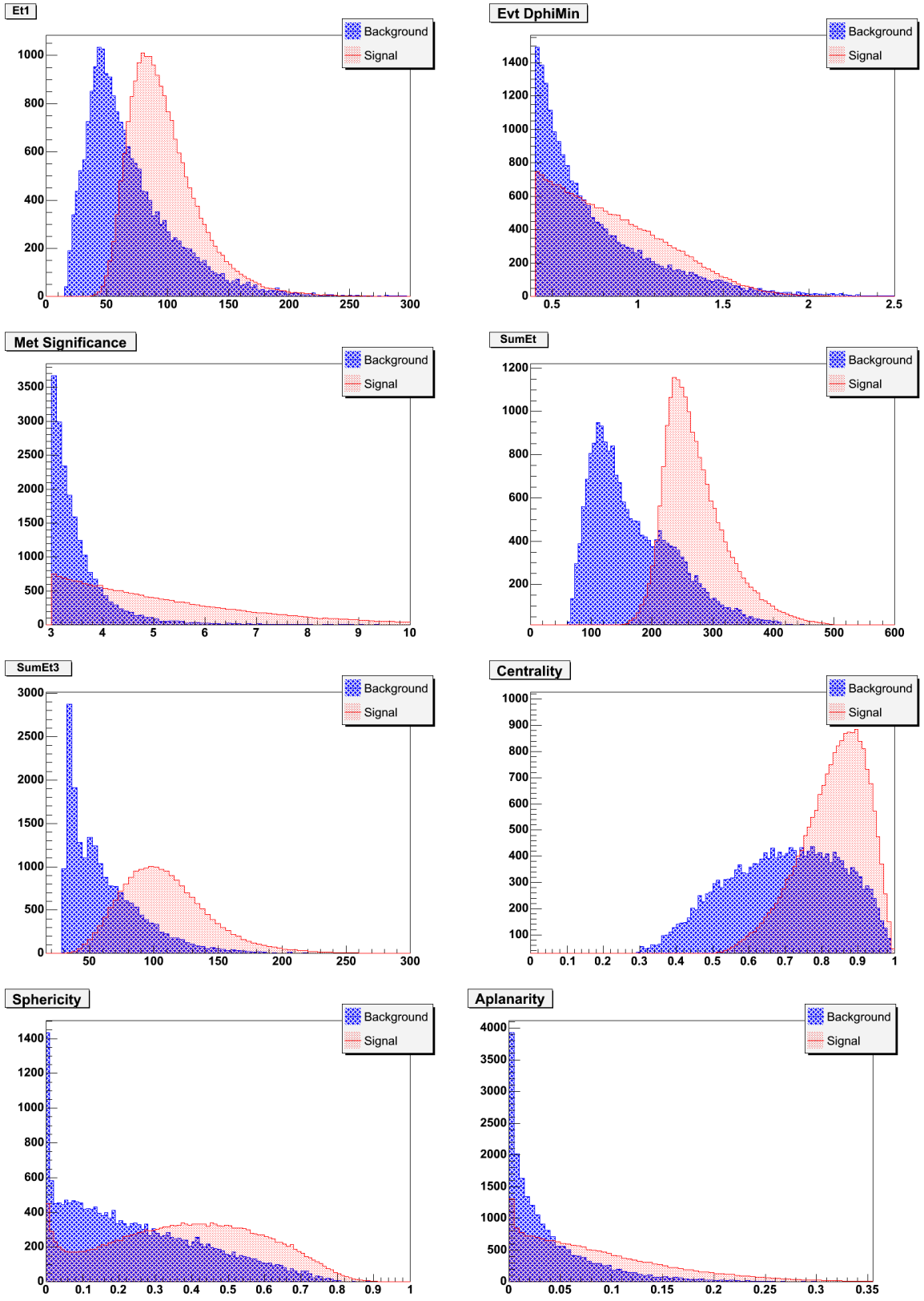

Figure 9: Distribution of neural network input variables for top multi jet data (background) and $t\bar{t}$ Monte Carlo (signal) samples, after prerequisites application (see text for details).

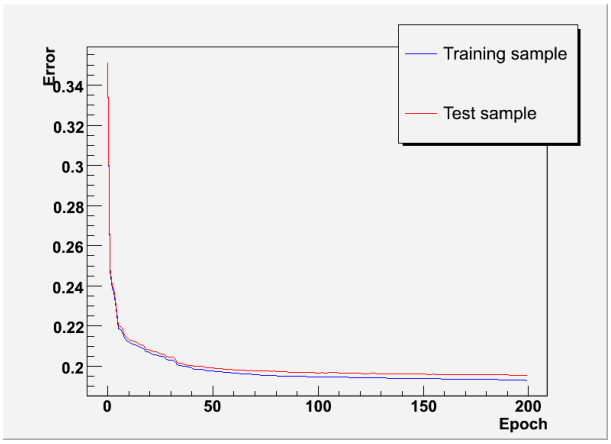

Figure 10: Average neural network error during training on training and test samples.

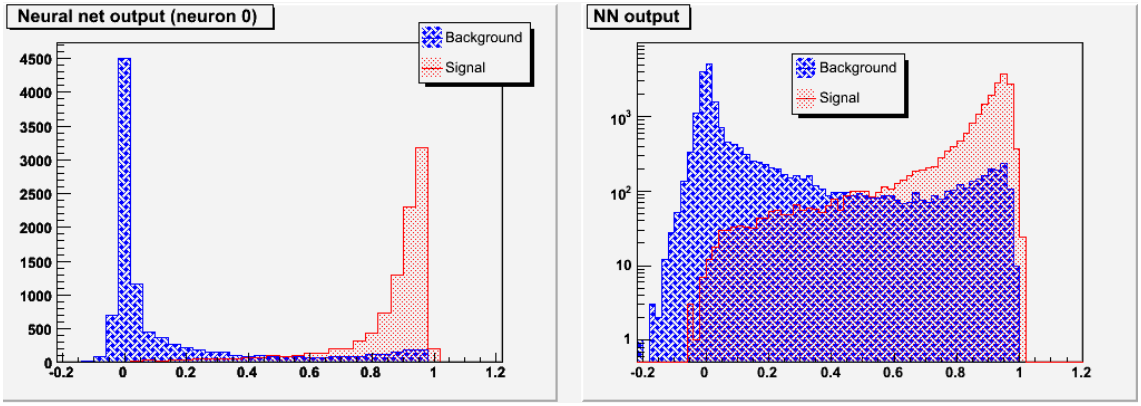

Figure 11: Output of the neural network after the training, right figure shows the same plot in log scale.

purity, defined as follows:

$$\epsilon(cut) = \frac{N_s^{pass}(cut)}{N_s}, \ \eta(cut) = \frac{N_s^{pass}(cut)}{N_s^{pass}(cut) + N_b^{pass}(cut)} \tag{6}$$

and $N_s^{pass}(cut)$ ($N_b^{pass}(cut)$) is the number of signal (background) events passing the cut on the neural network output (i.e. with $NNout >= cut$), and N_s is the total number of signal events in the test sample. Basically, purity describes how well a neural network can discriminate between signal and background, while efficiency is a measure of the neural network capability in recognizing signal events. An ideal neural network should have infinite precision in discriminating signal from background, so $\epsilon \approx 1$ and $\eta \approx 1$ and the efficiency vs. purity plot would be in this case a step function: the more the plot obtained after the training approaches the ideal one, the better the performances of the neural network.

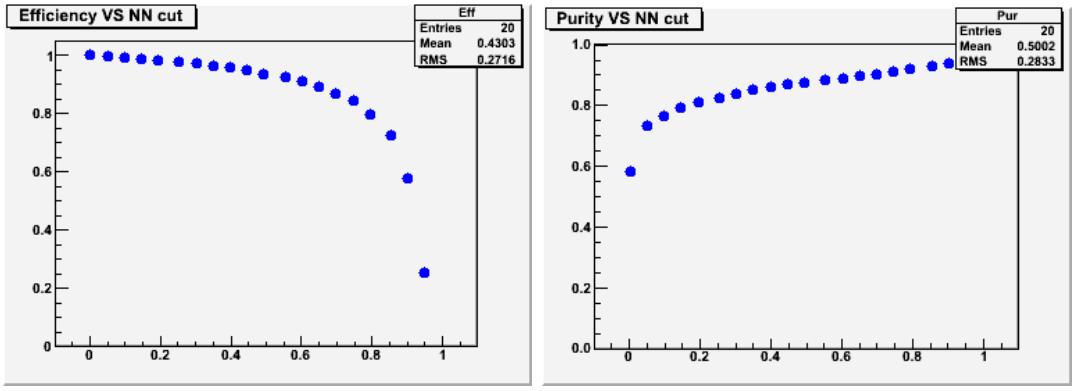

Figure 12: Performances of the Neural Network after training: efficiency vs cut on the output variable on top and purity vs cut on the output variable on the bottom.

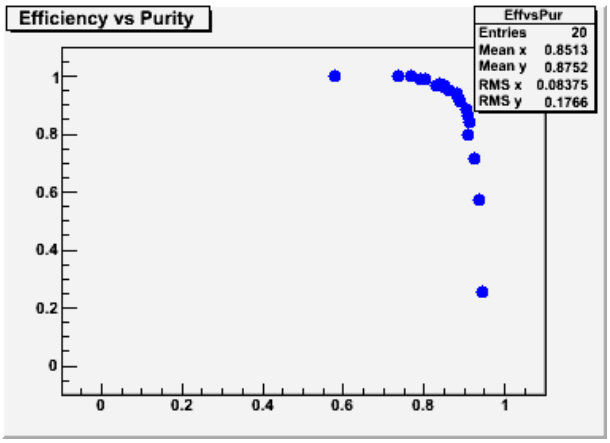

Figure 13: Efficiency versus Purity plot of the network obtained after the training.

As can be seen in Fig. 12, the efficiency of the network is good over all possible cuts on the output variable, while purity as a function of the cut on the output variable has a good trend, showing low background contamination for high cuts. We recall that the purity parameter does not refer directly to the purity of the final sample we will use for the cross section measurement: in fact it is just a measure of the performances of the network, being calculated submitting to the network a sample made of the same number of signal and background events. Finally, the efficiency versus purity plot approaches quite well the ideal "step" one, as shown in Fig. 13.

Another important variable we can use to characterize the neural network obtained after the training is the impact of each different input variable on the output of the network itself. A way to estimate this quantity is the following: we choose a fixed input variable α and, for each event, while keeping all the other input variables untouched, we shift the value of the α_i input by $\pm\frac{1}{10} \cdot RMS$, where RMS denotes the root mean

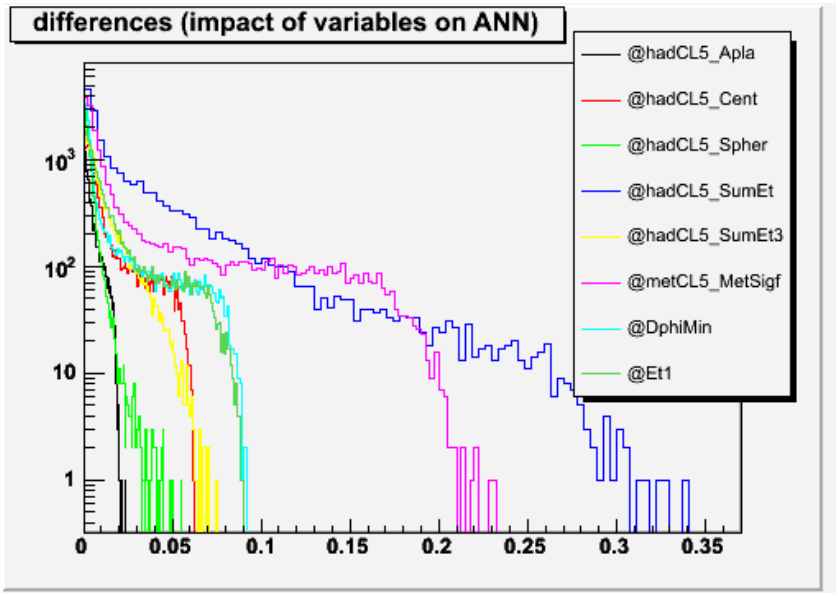

Figure 14: Impact of the input variables on the output of the neural network (see text for details).

square ($\sqrt{\sum_i \alpha_i^2}$) of that input variable calculated over all events submitted to the network. The output of the network after the shift of this single input is calculated and then compared to the output of the network without the shift. Finally, the square root of the difference of the squares of the 2 outputs is calculated and then used to fill an histogram. This is repeated for every variable and for each event in the sample, and provides a way to quantify how the output of the network depends on the fluctuations of each single input variable. The result of this procedure is shown in Fig. 14: it is easy to notice how $\sum E_T$ and $\not\!\!E_T{}^{sig}$ variations have the most determinant impact on the output of the network.

6.2.1 *b*-tagging rate extrapolation and Neural Network

An additional check we want to perform is related to the behaviour of the matrix predictions with respect to the output of the Neural Network we will use later for our kinematical selection; we want to verify that the prediction of the background works well over all the spectrum of the output of the neural network. Fig. 15 shows the output of the Neural Network and the corresponding background prediction from the tag matrix and the expected contribution from $t\bar{t}$ signal both for events with at least three tight jets and exactly three, four and five tight jets. Matrix predicted tags for bins with a considerable amount of signal contamination have been corrected according to the iterative procedure described in Sec. 5.3.3.

Results are quite good over all the neural network spectrum, altough some discrepancies arise mainly in the low output region. In the high neural network output region

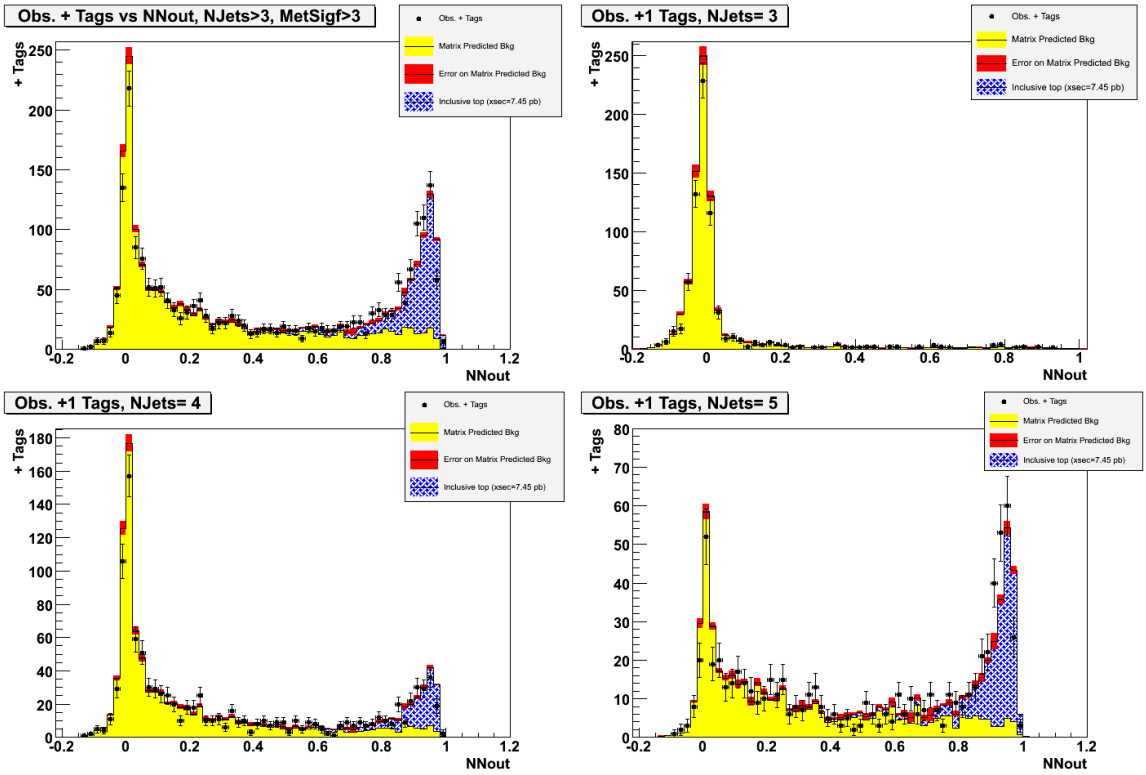

Figure 15: Tagging matrix check after prerequisites application and before any kinematical selection. Observed and predicted positive b-tags as a function of Neural Network output. Upper left plot shows the predictions for data events with at least three tight jets. The other plots refer to data events with exactly three (upper right), four (lower left) and five (lower right) tight jets.

we can see that the tagging matrix predictions are not sufficient to justify the number of observed tags, while the agreement is good if we add the amount of tags coming from the expected $t\bar{t}$ signal contribution. This is both a confirmation of the effectiveness of the method we used to estimate the background and an additional check of the correct behaviour of the neural network we trained.

As expected, agreement is very good in the 3 jets sample and this provides an additional check of the fact that the matrix parameterization is not affected by the application of the neural network. Furthermore, since we don't expect a sizeable signal presence in the sample, the fact that the vast majority of 3 jet events has a neural network output close to zero is again an indication of a well trained network.

7 Systematic Errors

7.1 Background prediction systematic

The systematic uncertainty on the background prediction is calculated by comparing the number of b-tags yelded by the tagging matrix application to the actual number of observed positive SECVTX tags in a control sample depleted of signal contamination (we choose the one with $NNout \leq 0.6$). The observed number of tags in this sample is 14870, while the tag matrix prediction is of 14792 ± 312.4, giving a ratio $|N_{Exp} - N_{Obs}|/N_{Obs} < 1\%$.

Considering the obs/exp b-tag ratio as a function of the jet multiplicity , we obtain the results of Tab. 6.

Number of +1 Tags	3 jets	4 jets	5 jets	6 jets	7 jets	8 jets
Observed	3074	6159	3819	1345	405	68
Mtx predicted	3086.7	6168.1	3726.2	1360.4	371.8	79.5
Error (stat.)	57.0	129.3	89.4	35.5	13.5	3.6
$\lvert N_{Exp} - N_{Obs}\rvert/N_{Obs}$ ratio (%)	0.41	0.15	2.5	1.2	8.2	17

Table 6: Difference between observed and matrix predicted +1 Tags for different jet multiplicities in the data sample with $NNout \leq 0.6$.

By calculating the weighed average of the errors in each bin, weighing each error by the number of + Tags observed in that jet multiplicity sample so that our result is not dominated by low statistics bins, we obtain an error $< 2\%$. We also note that the high statistics jet multiplicity sample with the largest error is for $NJets = 5$ and has an error of $\sim 2.5\%$.

The overall discrepancy between observed and matrix predicted number of b-tags due to intrinsic limits of the matrix and to the dependance from the sample in which the matrix has been built can then be quoted conservatively at 2.5%. This value will be assumed as the systematics uncertainty to be associated to our background prediction.

7.2 Luminosity systematic

Two components of uncertainty play a role in the luminosity measurement determination: the acceptance and operation of the luminosity monitor (the CLC detector) and the theoretical uncertainty of the total inelastic $p\bar{p}$ cross section (60.7 ± 2.4 mb). The uncertainties on these quantities are 4.2% and 4.0% respectively, giving a total uncertainty of 5.8% on the integrated luminosity calculated for any given CDF dataset [9].

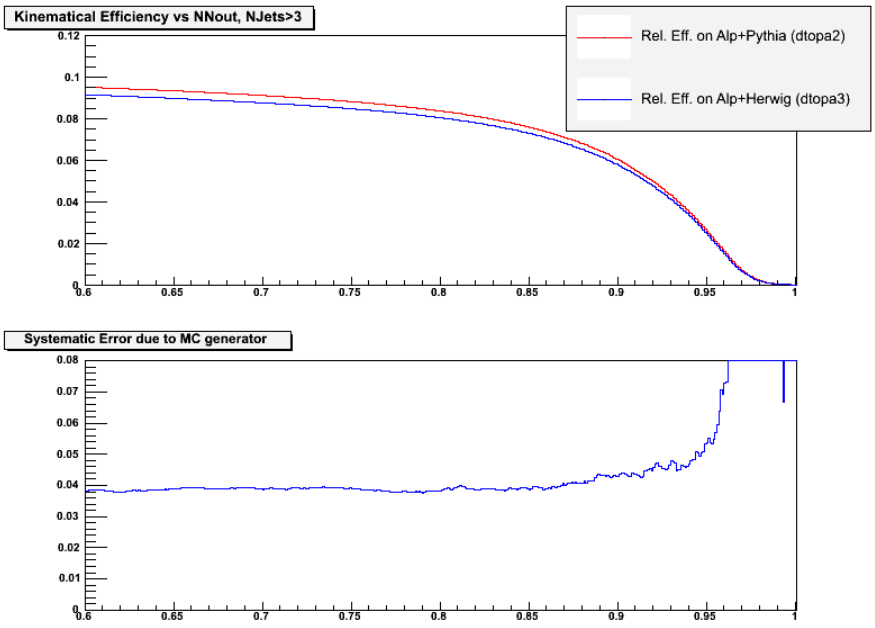

Figure 16: Top: relative kinematical efficiency of prerequisites and neural network selection versus cut applied on neural network output for both ALPGEN+PYTHIA Monte Carlo sample (dtopa2) and ALPGEN+HERWIG sample (dtopa3) generated at $M_{top} = 172.5\ GeV/c^2$. Bottom: Monte Carlo generator dependent systematic versus cut on neural network output. The error peak for neural network output cuts close to 1 is due to low statistics effects.

7.3 Monte Carlo generator dependent systematics

The base Monte Carlo sample adopted for this work is *ttop25* dataset generated using PYTHIA assuming $M_{top} = 172.5$ GeV. In order to evaluate the generator dependence of the kinematical efficiency computed for signal events we use two $t\bar{t}$ samples (*dtopa2* and *dtopa3*) generated with ALPGEN+PYTHIA and ALPGEN+HERWIG for the same top mass $M_{top} = 172.5$ GeV.

Since the ALPGEN+HERWIG sample was generated without QED FSR, we expect lepton ID to have higher efficiency on this sample. This causes our tight lepton veto prerequisite to have a lower efficiency on the ALPGEN+HERWIG sample.

We correct for this effect following the prescription available in [10]. We compare the relative efficiency on the two samples, defined as:

$$\epsilon^{rel}(cut) = \frac{N_{evts} \text{ passing cut NNout} \geq cut}{N_{evts} \text{ passing tight lepton veto prerequisite}} \tag{7}$$

The overall systematic uncertainty to be assigned to generator effects can then be computed for each neural network output cut as:

$$syst_{gen}(cut) = \frac{\Delta\epsilon^{rel}(cut)}{\epsilon^{rel}(cut)} = \frac{|\epsilon^{rel}_{HERWIG}(cut) - \epsilon^{rel}_{PYTHIA}(cut)|}{\epsilon^{rel}_{PYTHIA}(cut)} \tag{8}$$

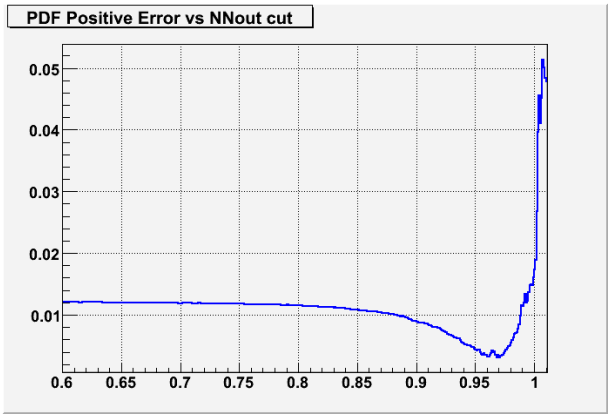

Figure 17: PDF dependent systematic, obtained with Monte Carlo reweighting tecnique, versus cut on neural network output. The error increases for neural network output cuts close to 1 because of low statistics effects.

where $\epsilon^{rel}_{PYTHIA}(cut)$ and $\epsilon^{rel}_{HERWIG}(cut)$ are the relative kinematical efficiencies for the chosen cut on $t\bar{t}$ inclusive Monte Carlo events generated with PYTHIA and HERWIG, respectively.

Fig. 16 shows the results of this calculation in the $0.6 - 1.0$ neural network output cut range.

7.4 PDF-related systematics

The parton distribution functions (PDFs) chosen for the standard CDF Monte Carlo generation correspond to the CTEQ parameterization outlined in [11]. There are uncertainties associated with this parameterization, since the usage of different parameterizations of the PDFs could slightly change the kinematics and thus the acceptance for signal events.

In order to account for these effects, we used a standard Monte Carlo reweighting tecnique. Instead of generating new samples for each different PDF, we re-weighted the events already generated with PYTHIA according to different PDF eigenvectors. The weight for each event is calculated as the ratio of the new PDFs with respect to the standard one. We then sum the weights in order to determine the effect on the total kinematic efficiency [12].

The results of the calculation for neural network output cuts in the range $0.6 - 1.0$ are shown in Fig. 17.

7.5 ISR/FSR-related systematics

In general it is very difficult for Monte Carlo generators to model accurately initial and final state radiation processes. If more or less extra radiation is present in the event with respect to the default values set in the base Monte Carlo sample, the event kinematics

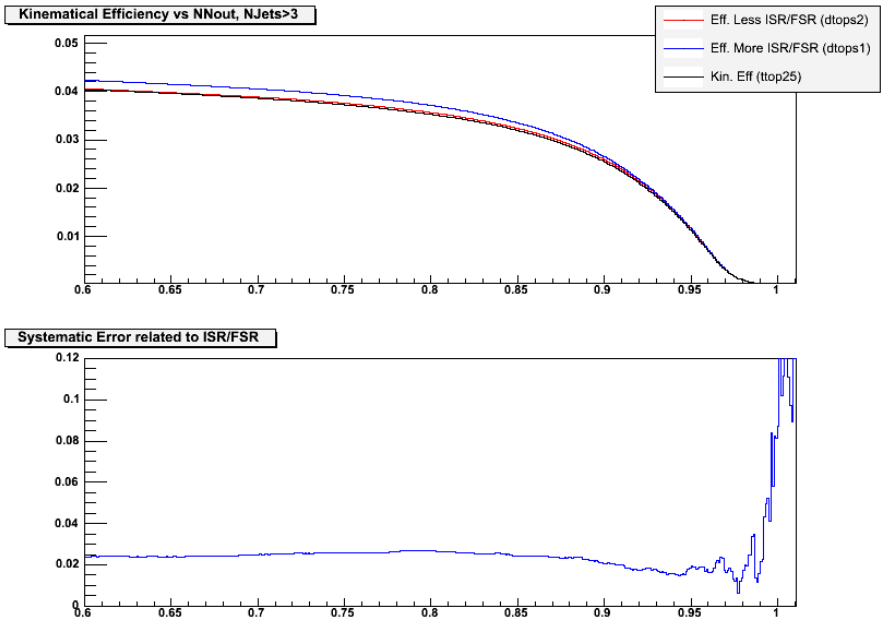

Figure 18: Top: kinematical efficiency of trigger, prerequisites and neural network selection versus cut applied on neural network output for PYTHIA Monte Carlo sample (ttop25) and samples generated with more and less initial/final state radiation. Bottom: Initial/Final state radiation systematic uncertainty versus cut on neural network output. The behaviour of the error function for neural network output cuts in the region close to 1 is due to low statistics effects.

could change affecting the kinematic efficiency determination. Indeed the presence of less or more radiation associated to the $t\bar{t}$ production can alter the acceptance of the N_{jet} and $\not\!\!E_T/\sqrt{\Sigma E_T}$ requirements.

We evaluated this effect using different inclusive Monte Carlo $t\bar{t}$ samples generated with different tunings for initial (ISR) and final state (FSR) radiation: less ISR/FSR (dtops2), and more ISR/FSR (dtops1).

We calculate systematic effects for each cut on neural network output as follows:

$$syst_{ISR/FSR}(cut) = \frac{|\epsilon_{+ISR/FSR}(cut) - \epsilon_{-ISR/FSR}(cut)|}{2\epsilon_{PYTHIA}(cut)} \tag{9}$$

when our nominal value for the kinematical efficiency $\epsilon_{PYTHIA}(cut)$ is in between the values $\epsilon_{+ISR/FSR}(cut)$ and $\epsilon_{-ISR/FSR}(cut)$ we use for comparison; when it is not, we will use half the maximum difference:

$$syst_{ISR/FSR}(cut) = \frac{max\left(|\epsilon_{+ISR/FSR}(cut) - \epsilon_{PYTHIA}(cut)|, |\epsilon_{PYTHIA}(cut)\epsilon_{-ISR/FSR}(cut)|\right)}{2\epsilon_{PYTHIA}(cut)} \tag{10}$$

Fig. 18 shows the results of this calculation in the $0.6 - 1.0$ neural network output cut range for both the ISR and FSR contributions respectively.

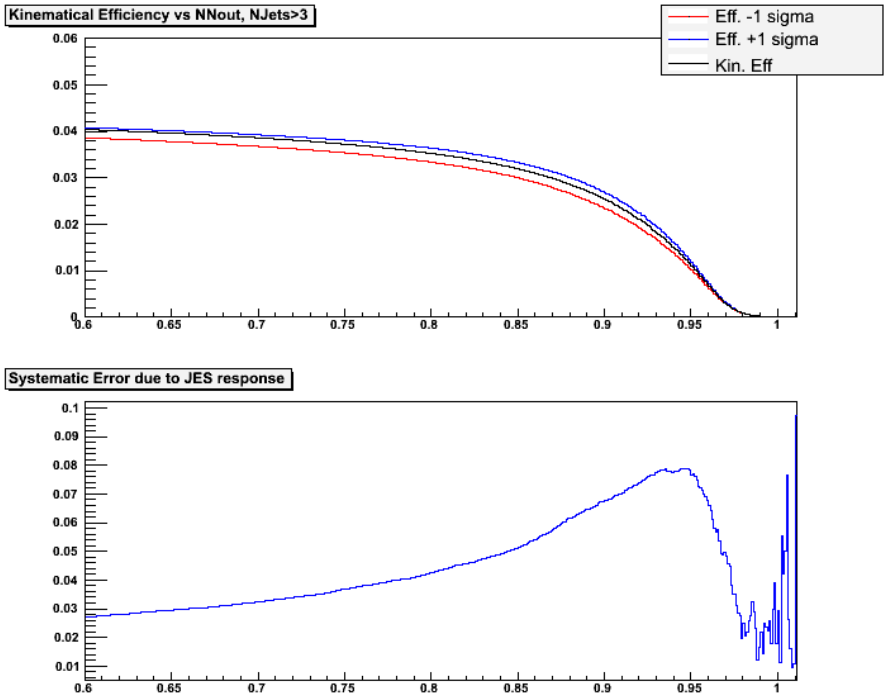

Figure 19: Top: kinematical efficiency of trigger, prerequisites and neural network selection versus cut applied on neural network output for the Monte Carlo sample (ttop25) with standard jet corrections and with jet energy corrections shifted by $\pm\sigma$ of their systematic error. Bottom: Systematic uncertainty due to jet energy repsonse versus cut applied on neural network output. In the neural network output cut region close to 1 low statistics effects arise, causing the error to increase.

7.6 Systematics due to the jet energy response

In order to account for the jet response systematic in the cross section measurement, we varied the corrected jet energies within $\pm 1\sigma$ of their corresponding systematic uncertainty. Therefore, signal trigger and prerequisites efficiencies are recalculated after these variations.

We can assign a systematic uncertainty depending on the cut we apply on the neural network output as follows:

$$syst_{jetcorr}(cut) = \frac{|\epsilon_{jetcorr,+1\sigma}(cut) - \epsilon_{jetcorr,-1\sigma}(cut)|}{2\epsilon_{kin}(cut)} \tag{11}$$

when our nominal value for the kinematical efficiency $\epsilon_{kin}(cut)$ is in between the values $\epsilon_{jetcorr,+1\sigma}(cut)$ and $\epsilon_{jetcorr,-1\sigma}(cut)$, while in the other case we will use half the maximum difference defined according to Eq. 10.

Fig. 19 show the results of this calculation in the $0.6 - 1.0$ neural network output cut range.

7.7 b-tagging scale factor systematics

The SECVTX efficiency scale factor we use in this analysis, to count the number of b-tags on Monte Carlo events, is $SF = 0.95 \pm 0.050$. Since the average number of b-tags per $t\bar{t}$ event, ϵ_{tag}^{ave}, enters directly in the cross section measurement we have to compute the systematics effect related to its determination.

To account for the scale factor uncertainty we varied it from its central value of 0.95 within the $\pm 1\sigma$ range and we determined the difference in terms of average number of b-tags per event on the Monte Carlo sample with respect to the standard value, taking into account that the SECVTX scale factor has the same central value for both b- and c-quarks, but for the latter has a doubled uncertainty: $SF_b = 0.95 \pm 0.050$, $SF_c = 0.95 \pm 0.100$.

For each cut on neural network output we can assign the following systematic uncertainty:

$$syst_{\epsilon_{tag}}(cut) = \frac{|\epsilon_{tag,+1\sigma}(cut) - \epsilon_{tag,-1\sigma}(cut)|}{2\epsilon_{tag}^{ave}(cut)} \tag{12}$$

The results are shown in Fig. 20. As expected, the systematic uncertainty due to the scale factor application does not depend much on the choice of the cut on the network output, since it only rescales the number of positive tags in a given sample.

7.8 Color reconnection systematics

Uncertainties arising from the modeling of color reconnections effects are estimated by comparing the kinematical efficiency of our cuts using Monte Carlo samples PYTHIA *ctopsd* and PYTHIA *ctopse*, both with $M_{top} = 172.5\ GeV$. These samples are generated using PYTHIA v6.4.20 so that the former, with "tune Apro", is similar to the default sample *ttop25*, while the latter, with "tune ACRpro", includes an explicit color reconnections model [13].

For each cut on the neural network output we can assign the following systematic uncertainty:

$$syst_{color}(cut) = \frac{|\epsilon_{ctopse}(cut) - \epsilon_{ctopsd}(cut)|}{\epsilon_{kin}(cut)} \tag{13}$$

The results are shown in Fig. 21.

7.9 Trigger systematics

Altough a common aproach in many CDF analyses is to use a data driven turnon curve to simulate the trigger on the Monte Carlo (MC) sample used in the analysis, we had to use a complete simulation of the trigger requirements on the MC trigger variables available through TrigSim, as already discussed in Sec. 3.

This is due to the fact that multijets triggers are in general very difficult to model using a turnon curve. The TOP_MULTI_JET trigger involves multiple jets and SumEt, correlated to each other, and is therefore sensitive to the event topology; as a result,

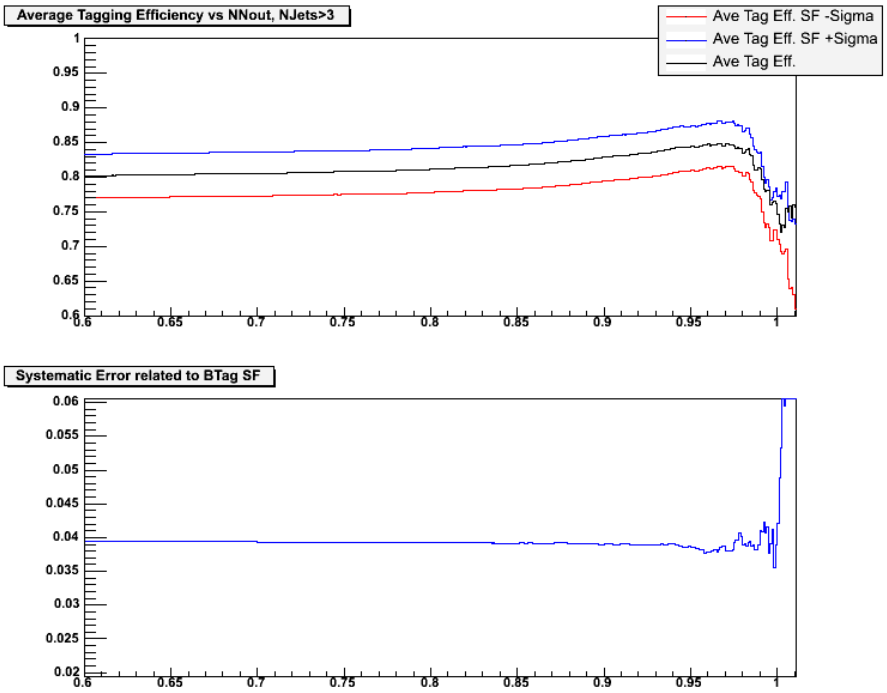

Figure 20: Top: Average tagging efficiency in the sample obtained after trigger, prerequisites and neural network selection versus cut applied on neural network output for the Monte Carlo sample (ttop25) with standard b-tagging Scale Factor and with Scale Factor shifted by $\pm\sigma$ of its systematic error. Bottom: Systematic uncertainty due to b-tagging scale factor application versus cut applied on neural network output. The behaviour of the error function in the output region close to 1 is due to low statistic effects.

trigger turnons are sample dependent. Therefore we cannot use a turnon curve derived from data to reweigh Monte Carlo events.

This problem has a direct effect on the method used to calculate trigger systematics. A first attempt to derive the trigger systematics would be to compare turnon curves in ttop25 Monte Carlo to those found in SingleTower10 data. SingleTower10 is an optimal candidate to derive the L2 TOP_MULTI_JET trigger turnon, since it shares the same L1 requirement as the TOP_MULTI_JET trigger itself, has a static prescale at L2 and auto-accept at L3, as already discussed in Sec. 3. Additionally, since we alredy know that this trigger is mainly driven by its L2 requirements [2], we can limit our systematics calculation to the L2 turnon.

Fig. 22 shows the L2 turnons calculated in the samples ttop25 (Monte Carlo) and SingleTower10 (data) with respect to the variable offline SumEt, L5 corrected. Events in the ttop25 sample are required to pass analysis prerequisites and to have at least 4 *tight* jets (i.e. jets with $E_T^{L5} \geq 15\ GeV$ and $|\eta| \leq 2.0$). Due to lower statistics, events in the SingleTower10 sample are required only to have at least 4 tight jets.

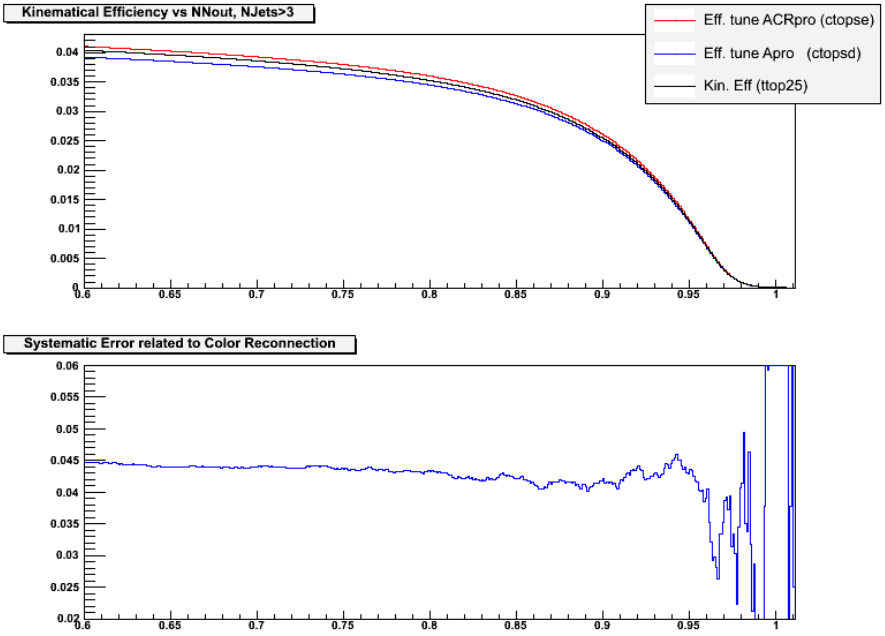

Figure 21: Top: kinematical efficiency of trigger, prerequisites and neural network selection versus cut applied on neural network output for the Monte Carlo sample (ttop25) used in the analysis compared with Pythia "tune Apro" (ctopsd) and with Pythia "tune ACRpro" (ctopse) simulations for $M_{top} = 172.5\ GeV$. Bottom: Systematic uncertainty due to color reconnection effects versus cut applied on neural network output. The behaviour of the error function in the output region close to 1 is due to low statistic effects.

The turnons show many differences: altough the L2_SUMET175 requirement turnon matches quite well in the two samples, the L2_FOUR_JET15 turnon is completely different, because of the differences in the physics of the two samples. Obviously this affects the overall L2_TOP_MULTI_JET turnon, which involves both the requirements.

By this comparison alone it's difficult to get sensible information on the trigger simulation systematics. This tells us that if we want a reliable determination of the trigger systematics, we have to compare a Monte Carlo sample and a data sample with the same physics.

To quote a systematic error related to our trigger simulation, we refer to the extensive study performed in [1] by A. Mitra. We will repeat his studies with our choice of jets. The method relies on the comparison of turnon curves between QCD40 MC and JET50 data.

Both samples are required to pass the following prerequisites:

- Good Run (QCD Silicon v24)
- $|Z_{vertex}| < 60$ cm

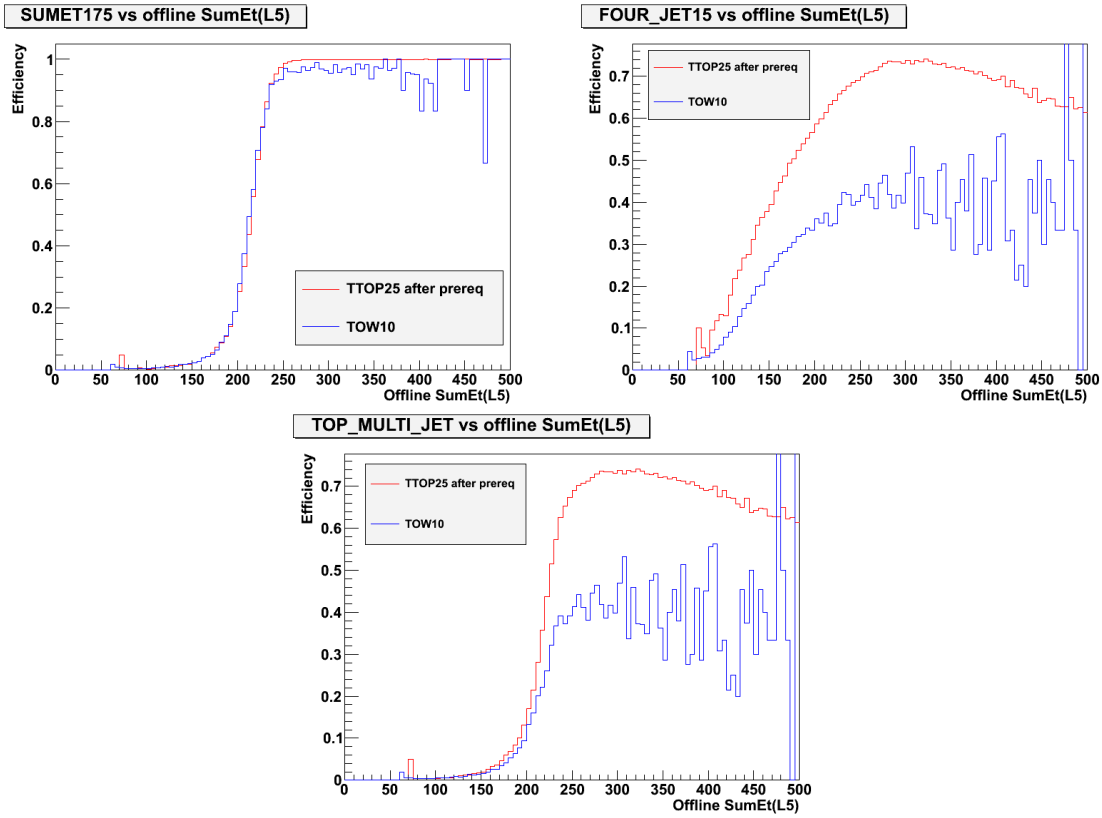

Figure 22: Comparison of the offline SumEt (L5 corrected) L2 turnon in the Monte Carlo sample ttop25 after analysis prerequisites versus the data sample SingleTower10. Both samples are required to have 4 or more tight jets. Upper left plot shows the turnon of the requirement L2_SUMET175 alone, upper right plot the turnon of the requirement L2_FOUR_JET15 alone, while the lower plot shows the turnon of the L2 TOP_MULTI_JET.

- Leading Jet $E_T > 60$ GeV
- At least 4 tight jets (i.e. cone 0.4 jets with $E_T^{L5} > 15$ GeV and $|\eta| < 2.0$)

We remind that we defined ΣE_T as the sum of the jet E_T over all tight jets in the event. To avoid any possible bias due to different kinematical properties of the two samples, we reweigh QCD40 events to have the same distributions of JET50 in the kinematical variables ΣE_T, Jet1 , Jet2, Jet3, Jet4 E_T and $min\Delta R$ among the jets.

To do so, we reweigh QCD40 events using a reweigh matrix defined as follows:

$$Mtx^{rwg}(E_T^{Jet1}, E_T^{Jet2}, E_T^{Jet3}, E_T^{Jet4}, \Sigma E_T, min\Delta R) = \\ = \frac{N_{evts}^{JET50}(E_T^{Jet1}, E_T^{Jet2}, E_T^{Jet3}, E_T^{Jet4}, \Sigma E_T, min\Delta R)}{N_{evts}^{QCD40}(E_T^{Jet1}, E_T^{Jet2}, E_T^{Jet3}, E_T^{Jet4}, \Sigma E_T, min\Delta R)}$$

Fig. 26 shows the behaviour of the chosen kinematical variables on JET50 data and on QCD40 before and after reweigh using the matrix we just defined.

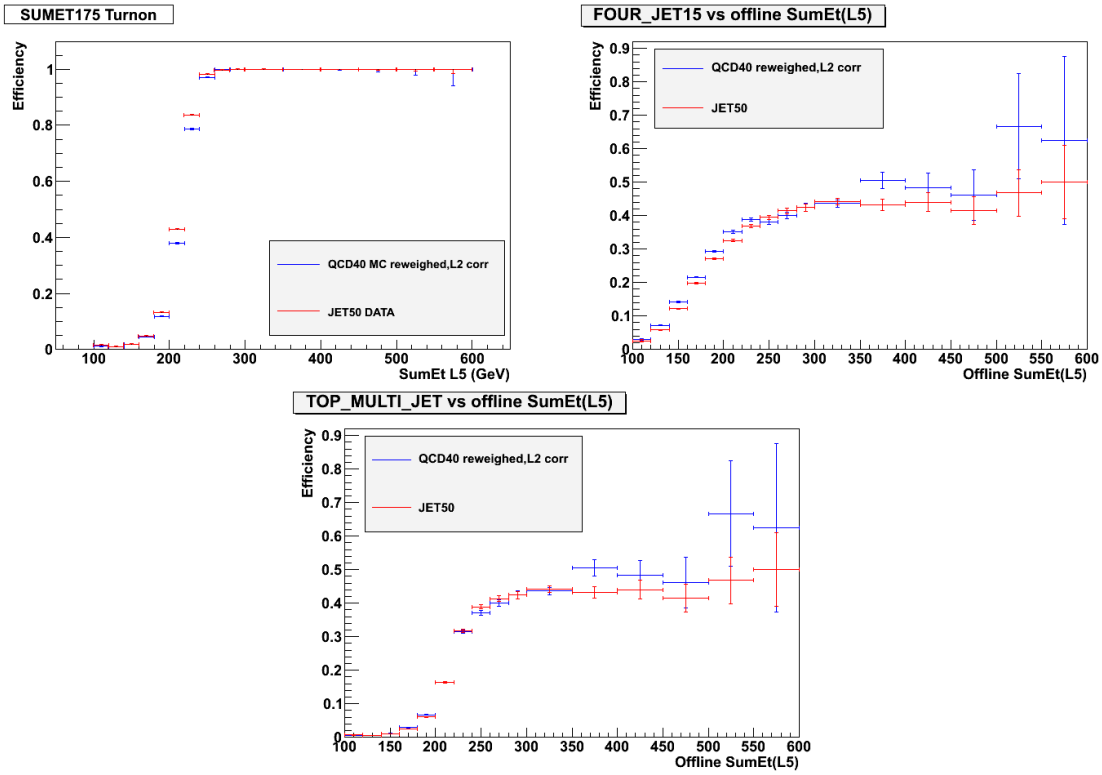

Figure 23: Comparison of the offline SumEt (L5 corrected) L2 turnon in the Monte Carlo sample QCD40 after reweigh and prerequisites versus the data sample JET50 after prerequisites. Both samples are required to have 4 or more tight jets. Upper left plot shows the turnon of the requirement L2_SUMET175 alone, upper right plot the turnon of the requirement L2_FOUR_JET15 alone, while the lower plot shows the turnon of the L2 TOP_MULTI_JET.

We can then calculate the L2 turnons in the JET50 data sample and in the reweighed QCD40 MC sample. The L2 trigger is simulated on the Monte Carlo sample QCD40 following the same method described in Sec. 3 for ttop25: we rescale the L2 cluster energies using A.Mitra's run dependent scale factors and then evaluate the different requirements. The results are shown in Fig. 23.

All the turnons match quite well, in particular the two TOP_MULTI_JET turnons; in order to derive the trigger systematics we fit the latter turnons with a sigmoid function. Fig. 24 shows the result of the fit of the two turnons.

Finally, we compute the systematic error following the same aproach of [4]. We compare in terms of distribution integrals simulated and real L2 turnon curves in the samples using the following formula:

$$\Delta\epsilon^{trg} = \frac{\int \mathcal{D}_{passL2}(\Sigma E_T)d\Sigma E_T - \int \mathcal{D}_{preL2}(\Sigma E_T) \times F^{turnon}_{jet50}(\Sigma E_T)d\Sigma E_T}{\int \mathcal{D}_{preL2}(\Sigma E_T)d\Sigma E_T} \qquad (14)$$

where $\mathcal{D}_{preL2}(\Sigma E_T)$ is the SumEt distribution of QCD40 events before any L2 re-

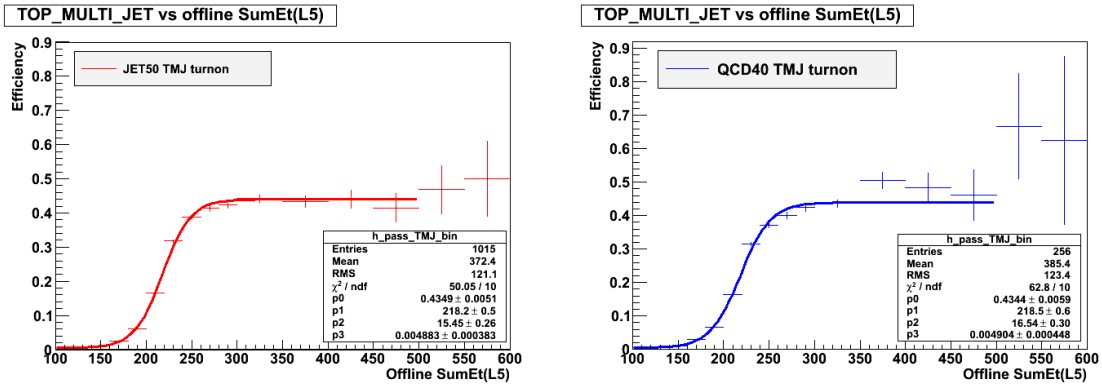

Figure 24: Fit of the JET50 data (left) and QCD40 MC (right) L2 TOP_MULTI_JET turnon.

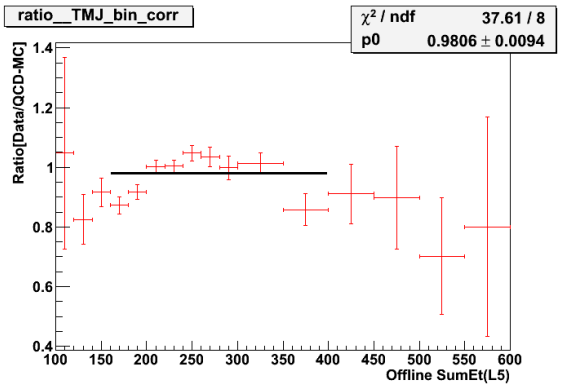

Figure 25: Fit of the bin by bin ratio of JET50 and QCD40 turnons, see text for details.

quirement, $\mathcal{D}_{passL2}(\Sigma E_T)$ is the SumEt distribution of QCD40 events passing L2, and $F^{turnon}_{jet50}(\Sigma E_T)$ is the SumEt TOP_MULTI_JET turnon derived from JET50 data. The resulting systematics on the efficiency is 2%.

The systematics we've just derived takes into account only the differences in normalization of the two turnons. To get an idea on how turnon shape differences can impact our analysis we check the Data/MC bin by bin ratio of the two turnons and then fit it with a straight line, excluding the regions where the turnon was obtained with less data. This method is used in [1].

Considering the bin by bin ratio, shown in Fig. 25, only the region with SumEt in the inerval 150-400 GeV could be fitted with a straight line, giving a difference in turnons of 2%, similar to the result we already found using the method of Eq. 14. The regions excluded from the fit have low statistics and contain only about 4% of ttop25 MC events after kinematical selection: so even if the difference in the turnons in this region is large (about 20%), the error in this region would affect our efficency with a systematics $< 1\%$. To be conservative, we quote an overall trigger systematics of 3%.

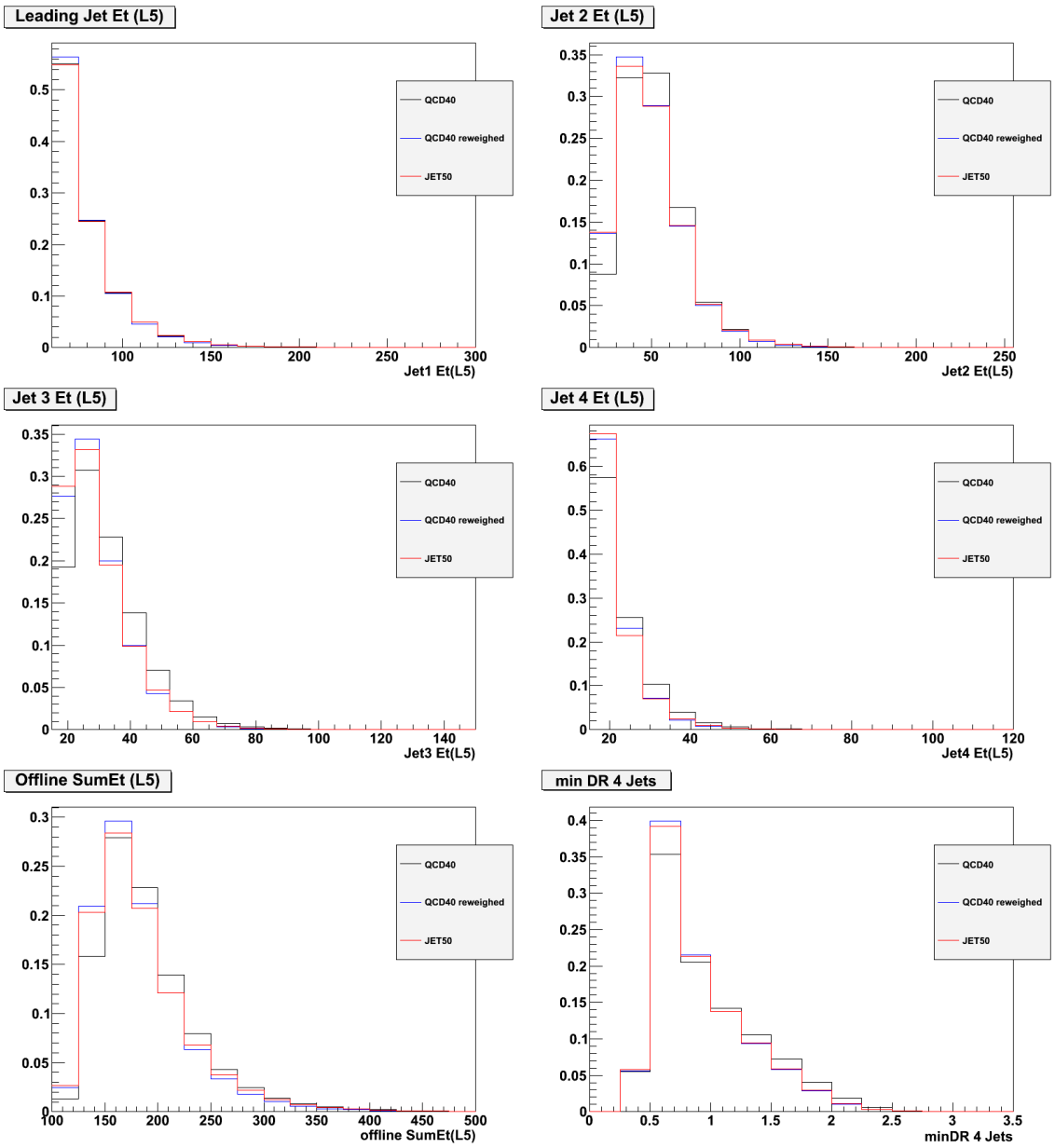

Figure 26: Kinematical distributions of JET50 data, QCD40 MC and QCD40 MC after reweigh. Plots from top to bottom, from left to right, show: leading Jet E_T, second, third and fourth Jet E_T, event $\sum E_T$ and $min\Delta R$ among the 4 leading jets in the event for the three samples.

8 NN cut optimization

Once we have trained the NN, we need to choose an optimized cut on the NN output to select the final data sample. The optimization procedure we seek is aimed at minimizing the statistical uncertainty on the cross section measurement, in order to optimize the measurement in terms of the expected number of b-tags over the background prediction. The former quantity is evaluated from inclusive Monte Carlo $t\bar{t}$ sample, the latter is derived from the b-tagging matrix application to data.

The optimization procedure for the event selection definition is performed after the $N_{jets} \geq 4$ requirement and scans different cuts on neural network output; among all possible cuts it chooses the one promising the minimum relative statistical error on the cross section measurement.

The central value of the production cross section we want to measure is given by:

$$\sigma(p\bar{p} \to t\bar{t}) \times BR(t\bar{t} \to \not{E}_T + jets) = \frac{N_{obs} - N_{exp}}{\epsilon_{kin} \cdot \epsilon_{tag}^{ave} \cdot L} \tag{15}$$

where N_{obs} and N_{exp} are the number of observed and matrix-predicted tagged jets in the selected sample, respectively; ϵ_{kin} is the trigger, prerequisites and neural network selection efficiency measured on inclusive Monte Carlo $t\bar{t}$ events; ϵ_{tag}^{ave}, defined as the ratio of the number of positive tagged jets to the number of pre-tagging events in the inclusive $t\bar{t}$ Monte Carlo sample, gives the average number of b-tags per $t\bar{t}$ event. Finally, L is the luminosity of the dataset used. Using in input to Equation 15 the measured kinematical efficiency, the average number of b-tags per $t\bar{t}$ event, the actual integrated luminosity and the number of b-tagged jet expected from the tag rate parameterization in the selected sample, we can estimate the expected cross section value and its relative statistical uncertainty for each neural network cut. The only missing piece is N_{obs}. We cannot use the actual number of observed b-tags in the selected data, since it would bias our conclusion given its possible statistical fluctuations. For this reason, in order to obtain an *a priori* determination of the best cut, we substitute N_{obs} with the expression $N_{exp} + N_{MC}$, where N_{exp} and N_{MC} are the number of expected b-tagged jets from the tagging rate application and from inclusive $t\bar{t}$ Monte Carlo samples after the application of the given neural network cut, respectively. Using these values, the statistical uncertainty affecting the measurement can be computed before looking at the "post-tagging" data sample, allowing in this way to choose the cut minimizing the relative error on the cross section measurement.

For each neural network output cut the following quantities are calculated:

- MC^{evt}, and $Data^{evt}$: number of inclusive Monte Carlo $t\bar{t}$ and data events in the selected sample, before any b-jet identification requirement.

- N_{MC} and N_{exp}: number of positive tags expected from Monte Carlo inclusive events and from tagging rate parameterization after the kinematical selection defined by the cut on the neural network output. Since we want to derive a "blind"

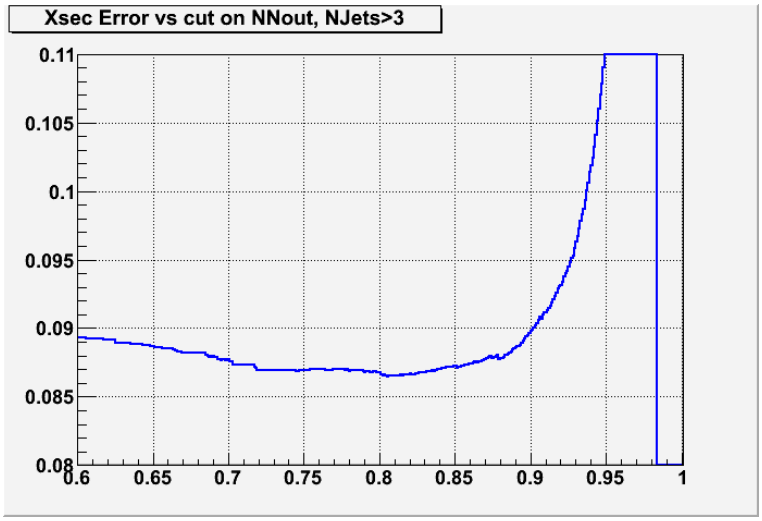

Figure 27: Expected statistical error as a function of the cut on the NN output. We decide to cut at $NNout \geq 0.8$

minimization procedure, we don't want to look at the post-tagging sample, meaning we won't use any information on the number of observed b-tags N_{obs} in the sample obtained after the neural network cut.

- ϵ_{kin} and ϵ_{tag}^{ave} are derived from the application of the cut to the Monte Carlo sample.

- the signal statistical significance obtained as $S/\sqrt{S+B}$: ratio of the number of tags expected for $t\bar{t}$ events and the square root of the number of tags expected from background processes plus the number of tags expected from signal.

- $\sigma_{xsec}/xsec$: relative error on the cross section measurement.

Results are reported in Fig. 27: we decide to cut at $NNout \geq 0.8$, which gives the lowest expected statistical error on the cross section (8.6%) and an expected S/B ratio in terms of positive tags of 4 (Fig. 28). To fix this cut we also check its effect on the total expected uncertainty and on the signal significance (Fig. 29). The total error (stat+syst) is $\sim$ 12% at $NNout = 0.8$ and it varies of only about 1% moving the cut below 0.8 (this determination includes only the contribution coming from systematic errors that depend on the chosen NN output cut, while it doesn't consider the background prediction systematics and the trigger systematics, which we assume to be constant in the scanned cut range). The signal significance is maximum and almost flat around $NNout = 0.8$.

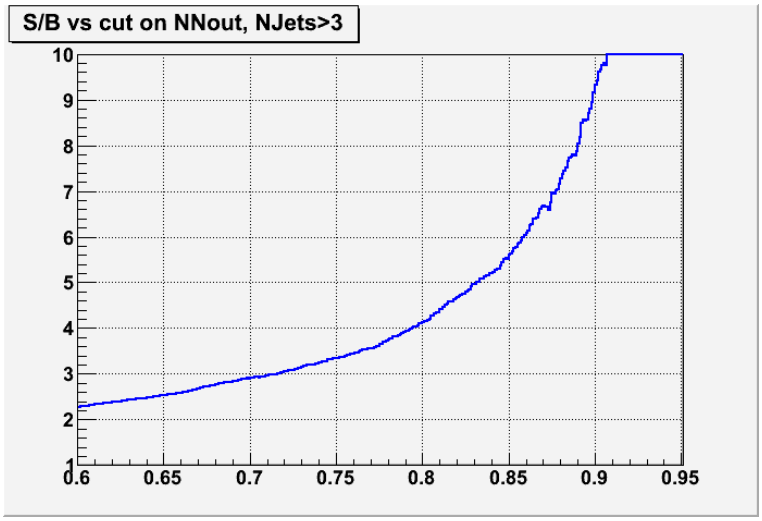

Figure 28: Signal to background ratio as a function of the cut on the NN output.

NJets	3	4	5	6	7	8	9	Tot.
allHad (%)	0.12	0.46	1.66	4.86	7.79	10.18	9.88	2.29
e +jets (%)	26.64	25.19	35.46	36.20	35.10	33.60	33.83	32.08
μ +jets (%)	32.16	32.51	19.09	15.78	14.46	16.08	12.87	22.71
dilepton (%)	6.46	2.30	1.07	0.70	0.52	0.64	0.00	1.45
had τ +jets (%)	15.79	21.86	30.53	31.49	31.85	29.86	34.43	27.73
lep τ +jets (%)	11.75	13.18	9.89	9.14	8.92	8.12	8.38	10.76
$\tau\tau$ (%)	1.06	1.15	0.65	0.47	0.43	0.44	0.30	0.77
$e/\mu + \tau$ (%)	6.03	3.36	1.64	1.35	0.92	1.08	0.30	2.16

Table 7: MC Sample Composition after NNout cut.

9 Cross Section Measurement

After our selection we are left with 1420 events with at least 4 tight jets and we observe 636 positive b-tags. Observed and expected positive b-tags after selection for different jet multiplicities are shown in Fig. 30.

The expected sample composition after this cut is shown in Tab. 7, while Tab. 8 shows the number of expected events for the different decay channels in 2.2 fb^{-1}.

Using the tagging rate parametrization applied to the 1420 events passing the selection, the background amount in terms of b-tagged jets is calculated to be $232.9 \pm 12.8(stat) \pm 5.8(syst)$, where the first uncertainty is statistical only, while the latter is systematic and is calculated by comparing observed to matrix-predicted b-tags in data control samples and quoting a 2.5% systematic uncertainty. This value needs to be corrected for the signal presence in the pre-tagging sample: the application of our iterative correction procedure yelds a top-free background determination of

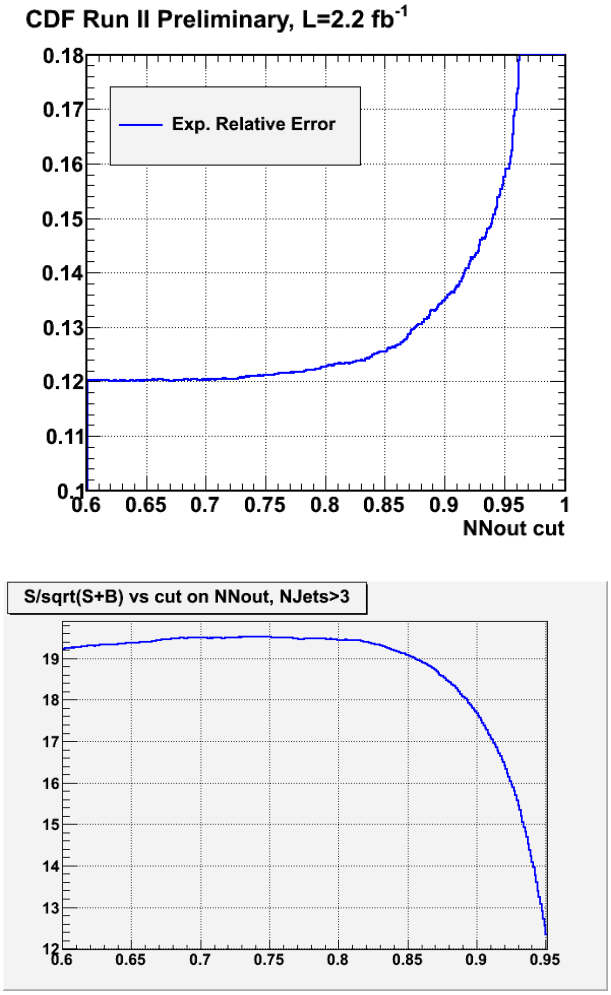

Figure 29: Up: total expected error as a function of the cut on the NN output. The tag matrix systematic and trigger systematics contributions are not included as they are considered costant as a function of the cut on NN out. Bottom: Signal signficance as a function of the cut on the NN output. The cut $NNout \geq 0.8$ maximizes the signal significance with a total expected error on the cross section of $\sim 12\%$.

$N_{exp}^{corr} = 131$. The uncertainty on the background correction depends both on the uncertainty on N_{exp} and the uncertainty on ϵ_{tag}^{ave}. In order to evaluate both contributions we follow the tecnique adopted in [8]: we generate $1,000,000$ random samples of N_{exp} events smeared with its statistical uncertainty and apply the iterative correction using ϵ_{tag}^{ave} smeared with its statistical uncertainty. The resulting N_{exp} distribution gives $N_{exp}^{corr} = 131 \pm 9$ (stat) ± 3.3 (syst).

The summary of all the sources of systematic uncertainty to the cross section evaluation is listed in Tab. 9 for the chosen cut $NNout \geq 0.8$.

Now that we have evaluated all the sources of systematic uncertainty affecting the kinematical selection efficiency as well as the determination of the average number of

NJets	3	4	5	6	7	8	9	Tot.
allHad	0.01	0.86	3.92	5.24	2.41	0.71	0.11	13.27
e +jets	2.34	47.24	83.55	39.01	10.88	2.35	0.39	185.75
μ +jets	2.82	60.96	44.98	17.00	4.48	1.12	0.15	131.51
dilepton	0.57	4.31	2.53	0.76	0.16	0.04	0.00	8.38
had τ +jets	1.38	40.99	71.92	33.94	9.87	2.09	0.40	160.58
lep τ +jets	1.03	24.71	23.29	9.86	2.77	0.57	0.10	62.32
$\tau\tau$	0.09	2.15	1.54	0.51	0.13	0.03	0.00	4.47
$e/\mu + \tau$	0.53	6.30	3.86	1.46	0.29	0.08	0.00	12.51
Tot.	8.77	187.53	235.59	107.78	30.99	6.98	1.15	578.79

Table 8: Expected Signal events in 2.2 fb^{-1} after NNout cut.

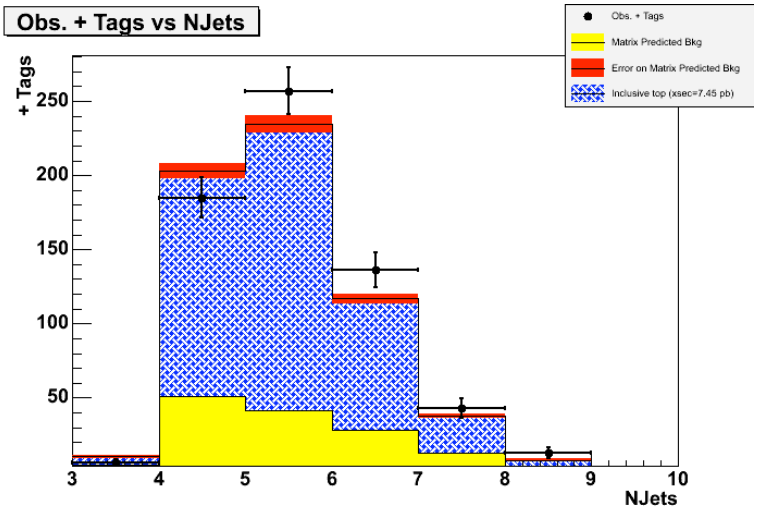

Figure 30: Number of positive tagged jets versus jet multiplicity. Data (points), iteratively corrected background (yellow histogram) and $t\bar{t}$ expectation (blue histogram) for $\sigma_{t\bar{t}} = 7.45$ pb are shown after neural network selection. Statistical errors only.

b-tags per $t\bar{t}$ event and the background prediction, we are ready to perform the cross section measurement.

We remind that we will interpret the excess in the number of tags defined as $N_{obs} - N_{exp}^{corr}$ as a sign of $t\bar{t}$ production and it will be used for the cross section measurement.

The value of the cross section is given by:

$$\sigma_{t\bar{t}} = \frac{N_{obs} - N_{exp}^{corr}}{\epsilon_{kin} \cdot \epsilon_{tag}^{ave} \cdot L} \tag{16}$$

The input parameters of Eq. 16 are quoted in Tab.10.

The measured cross section value is:

Source	Method	Uncertainty
ϵ_{kin} systematics		
Generator dependence	$\frac{\lvert\epsilon_{PYTHIA}-\epsilon_{HERWIG}\rvert}{\epsilon_{PYTHIA}}$	3.9 %
PDFs	MC reweighting	1.2 %
ISR/FSR	samples comparison	2.7 %
Color Reconnection	samples comparison	4.3 %
Jet Energy Scale	$\frac{\lvert\epsilon_{jetcorr,+1\sigma}-\epsilon_{jetcorr,-1\sigma}\rvert}{2\epsilon_{kin}}$	4.2 %
Trigger simulation	turn-on curves	3.0 %
Primary Vertex $Z0$		0.2 %
ϵ_{tag} systematics		
SecVtX scale factor	$\frac{\lvert\epsilon_{tag,+1\sigma}-\epsilon_{tag,-1\sigma}\rvert}{2\epsilon_{tag}}$	3.9 %
Tagging matrix systematics		
Data control sample	N_{obs}/N_{exp}	2.5 %
Luminosity systematics		
Luminosity measurement	–	5.8 %

Table 9: Summary of the sources of systematic uncertainty.

Variable	Symbol	Value
Integrated Luminosity (pb^{-1})	$\mathcal{L}$	2207.5 ± 128
Observed Tags	N_{obs}	636
Expected Background Tags	N_{exp}^{corr}	131 ± 9.6
Kin. efficiency (%)	ϵ_{kin}	3.53 ± 0.29
Ave. b-tagging efficiency	ϵ_{tag}^{ave}	0.811 ± 0.032

Table 10: Input values for the cross section measurement.

$$\begin{aligned}\sigma_{t\bar{t}} &= 7.99 \pm 0.55\ (\text{stat}) \pm 0.76\ (\text{syst}) \pm 0.46\ (\text{lumi})\ pb \\ &= 7.99 \pm 1.05\ pb\end{aligned}$$

10 Summary

We presented a research aimed at the isolation of the $t\bar{t} \rightarrow \not\!\!E_T + jets$ signal by means of neural network tools from a dataset containing "multijet" triggered events with a total integrated luminosity amounting to 2.2 fb^{-1}.

The decay channel has been extracted using a neutrino signature such as the presence of high $\not\!\!E_T$ in the event and by explicitly vetoing well identified high-P_T electrons or muons from W boson decay.

A 2-hidden layers neural network trained with input variables related to jet characteristics and energy and event topology and energy has been used to classify and discriminate between top-like events obtained from a Monte Carlo sample generated at $M_{top} = 172.5\ GeV/c^2$ and background processes contained in the data sample after prerequisites requirements.

Secondary vertex b-tagging algorithm has been exploited to indentify heavy flavour jets due to top quark decay, while the amount of tags coming from background processes has been evaluated by means of a parameterization of the b-tagging rate as a function of the jet transverse energy, jet number of tracks and projection of the $\not\!\!E_T$ of the event along the jet direction, in a data sample with negligible signal contamination containing exactly 3 tight jets.

Once checked the performance of the tagging parameterization and the correctness of its predictions, the optimized cut on the neural network output $NNout \geq 0.8$ has been computed by minimizing the relative statistical error on the cross section measurement.

With the resulting selection we obtained a pre-tagging sample of 1420 events: in order to derive our final cross section measurement, we added the requirement of the presence of at least one jet identified as originating from a b-quark, observing 636 b-tags. Thanks to our b-tagging rate parameterization we accounted for 131 ± 9.6 b-tags coming from $t\bar{t}$ events.

After taking into account the possible sources of systematics uncertainties and assuming a top quark mass of 172.5 GeV/c^2, our final measurement of the top pair production cross section is:

$$\begin{aligned} \sigma_{t\bar{t}} &= 7.99 \ \pm 0.55 \text{ (stat)} \ \pm 0.76 \text{ (syst)} \ \pm 0.46 \text{ (lumi) } pb \\ &= 7.99 \ \pm 1.05 \ pb \end{aligned}$$

in agreement with Standard Model predictions and with previous determinations. Moreover, being derived from a data sample that was chosen by prerequisites to be orthogonal to the ones used for the other cross section determinations at CDF, this measurement promises to be particularly important in the combination of the results obtained by the experiment.

11 Bibliography

References

[1] A. Mitra, Multijet Triggers for All-Hadronic Higgs Channel.

[2] A. Mitra *et al.*, *Study of the Top Multijet Trigger Efficiency for the Search of the Standard Model Higgs Boson*, CDF Note 9252.

[3] K. Copic and M. Tecchio, *Event vertex studies for dilepton events*, CDF Note 6933.

[4] G. Cortiana *et al.*, *Measurement of the $t\bar{t}$ production cross section in the $\tau + jets$ channel with SecVtX tags using $311pb^{-1}$ of $p\bar{p}$ data*, CDF Note 7689.

[5] A. Abulencia *et al.* [CDF Collaboration], *Measurement of the $t\bar{t}$ production cross section in $p\bar{p}$ collisions at $\sqrt{s} = 1.96\ TeV$ using $\not\!\!E_T + jets$ events with secondary vertex b-tagging*, *Phys. Rev. Lett.* **96** (2006) 202002.

[6] G. Cortiana *et al.*, *t tbar $\rightarrow$ tau + jets nt5 analysis update*, CDF Note 7553.

[7] G. Cortiana *et al.*, *Background studies for the $t\bar{t} \rightarrow \tau + jets$ search*, CDF Note 7292.

[8] A. Castro *et al.*, *Top Production Cross Section in the all-hadronic channel*, CDF Note 3464.

[9] S. Jindariani *et al.*, *Luminosity Uncertainty for Run 2 up until August 2004*, CDF Note 7446.

[10] A. Varganov, Understanding $t\bar{t}$ generator systematics.

[11] J. Pumplin *et al.*, *New generation of parton distributions with uncertainties from global QCD analysis*, *J. High Energy Phys.* **0207** (2002) 012

[12] O. Gonzalez *et al.*, *Uncertainties due to PDFs for the gluino-sbottom search*, CDF Note 7051.

[13] P. Skands, D. Wicke, *Non-perturbative QCD effects and the Top Mass at the Tevatron*, arXiv:0807.3248 [hep-ph].